# Distinct self-interaction domains promote Multi Sex Combs accumulation in and formation of the *Drosophila* histone locus body

Esteban A. Terzo[a], Shawn M. Lyons[b], John S. Poulton[b], Brenda R. S. Temple[c], William F. Marzluff[a,b,c,d,e], and Robert J. Duronio[a,b,d,e,f]

[a]Curriculum in Genetics and Molecular Biology, [b]Department of Biology, [c]Department of Biochemistry and Biophysics, [d]Lineberger Comprehensive Cancer Center, [e]Integrative Program for Biological and Genome Sciences, and [f]Department of Genetics, University of North Carolina, Chapel Hill, NC 27599

**ABSTRACT** **Nuclear bodies (NBs) are structures that concentrate proteins, RNAs, and ribonucleoproteins that perform functions essential to gene expression. How NBs assemble is not well understood. We studied the *Drosophila* histone locus body (HLB), a NB that concentrates factors required for histone mRNA biosynthesis at the replication-dependent histone gene locus. We coupled biochemical analysis with confocal imaging of both fixed and live tissues to demonstrate that the *Drosophila* Multi Sex Combs (Mxc) protein contains multiple domains necessary for HLB assembly. An important feature of this assembly process is the self-interaction of Mxc via two conserved N-terminal domains: a LisH domain and a novel self-interaction facilitator (SIF) domain immediately downstream of the LisH domain. Molecular modeling suggests that the LisH and SIF domains directly interact, and mutation of either the LisH or the SIF domain severely impairs Mxc function in vivo, resulting in reduced histone mRNA accumulation. A region of Mxc between amino acids 721 and 1481 is also necessary for HLB assembly independent of the LisH and SIF domains. Finally, the C-terminal 195 amino acids of Mxc are required for recruiting FLASH, an essential histone mRNA-processing factor, to the HLB. We conclude that multiple domains of the Mxc protein promote HLB assembly in order to concentrate factors required for histone mRNA biosynthesis.**

**Monitoring Editor**
Karsten Weis
ETH Zurich

Received: Oct 14, 2014
Revised: Feb 10, 2015
Accepted: Feb 12, 2015

## INTRODUCTION

Numerous levels of molecular organization within the nucleus facilitate the highly regulated expression of the genome. One level of organization is the concentration of proteins, RNAs, and ribonucleoproteins into structures known as nuclear bodies (NBs) that are visible by light microscopy (Matera, 1999; Matera *et al.*, 2009; Gall, 2000; Dundr and Misteli, 2001, 2010; Misteli, 2001, 2005; Parada *et al.*, 2004). NBs include well-known structures such as Cajal bodies and the nucleolus and less well understood structures including PML bodies, speckles, paraspeckles, and histone locus bodies (HLBs). An attractive hypothesis for NB function posits that NBs concentrate factors to accelerate reactions that would otherwise take longer if these factors were dispersed throughout the nucleus (Dundr, 2012). This hypothesis has gained support from studies of vertebrate Cajal bodies, which promote efficient spliceosomal small nuclear ribonucleoprotein (snRNP) assembly (Klingauf *et al.*, 2006; Strzelecka *et al.*, 2010; Novotny *et al.*, 2011; Machyna *et al.*, 2014). However, *Drosophila* snRNA modification by scaRNAs, which are localized to Cajal bodies, does not require Cajal body assembly (Deryusheva and Gall, 2009). Thus the general applicability and further tests of this hypothesis require additional study.

An understanding of NB function requires detailed knowledge of NB composition and assembly. We have been exploring this issue by studying how HLB assembly contributes to the expression of replication-dependent histone genes, which encode the only known cellular mRNAs that are not polyadenylated (Marzluff *et al.*, 2008). HLBs were defined by Gall and coworkers as NBs associated with

This article was published online ahead of print in MBoC in Press (http://www.molbiolcell.org/cgi/doi/10.1091/mbc.E14-10-1445) on February 18, 2015.
Address correspondence to: Robert J. Duronio (duronio@med.unc.edu).
Abbreviations used: FLASH, FADD-like interleukin-1β–converting enzyme/caspase-8–associated huge protein; LisH, lissencephaly type-1–like homology; Mute, muscle wasted; NB, nuclear body; PML, promyelocytic leukemia; scaRNA, small Cajal body–specific RNA; snRNA, small nuclear RNA.

the *Drosophila* histone gene locus that contained U7 snRNP (Liu *et al.*, 2006), a factor essential for generating the unique histone mRNA 3′ end (Strub and Birnstiel, 1986; Mowry and Steitz, 1987). Similar factors necessary for histone transcription and pre-mRNA processing are found in both vertebrate and *Drosophila* HLBs, including human nuclear protein mapped to the mutated ataxia telangiectasia locus (NPAT), which was identified as a cyclin E/Cdk2 substrate essential for histone mRNA expression (Ma *et al.*, 2000; Zhao *et al.*, 2000; Wei *et al.*, 2003; Miele *et al.*, 2005). The *multi sex combs* (*mxc*) locus encodes the *Drosophila* orthologue of NPAT. Mxc, like NPAT, is phosphorylated by cyclin E/Cdk2, colocalizes with U7 snRNP at the histone locus, and is required for both HLB assembly and histone gene expression (White *et al.*, 2011). Other known HLB components include FLASH and Mute. FLASH was identified in mammals as colocalizing with NPAT (Bongiorno-Borbone *et al.*, 2008) and subsequently shown to interact with U7 snRNP and be essential for histone pre-mRNA processing (Yang *et al.*, 2009). *Mute* was identified as a *Drosophila* HLB component in a screen for factors required for muscle development, but its biochemical function is not known (Bulchand *et al.*, 2010).

Our previous experiments on *Drosophila* HLBs suggest that Mxc is critical for HLB assembly. Mxc and FLASH localize to the histone locus immediately before the beginning of histone gene expression in syncytial embryos, and HLBs are not detected before this time. Loss of Mxc results in a failure to localize other HLB components, including FLASH and U7 snRNP (White *et al.*, 2011). The *Drosophila* HLB is present in all cells, independent of whether they are cycling (Liu *et al.*, 2006; White *et al.*, 2007). The five canonical *Drosophila* histone genes (H1, H2A, H2B, H3, and H4) are clustered together in a 5-kb sequence that is repeated ~100 times at a single locus on chromosome 2. The 300–base pair bidirectional promoter of the H3-H4 gene pair within this cluster is necessary and sufficient for HLB assembly and is necessary for expression of the adjacent H2A-H2B gene pair (Salzler *et al.*, 2013). This 300–base pair sequence is also sufficient to recruit Mxc and FLASH, consistent with Mxc playing an integral role in HLB assembly and histone gene expression. How Mxc participates in coordinating these processes remains unclear.

The *mxc* locus was originally described by an allelic series of mutations in which null alleles resulted in a failure of cell proliferation and lethality. Knocking out NPAT in cultured mammalian cells is similarly lethal (Ye *et al.*, 2003). In contrast, viable, hypomorphic *mxc* alleles cause homeotic transformations in adult males (giving rise to the gene name; Santamaria and Randsholt, 1995). Whether there is any causal relationship between histone gene expression and the homeotic transformations observed in *mxc* hypomorphs is unknown. Two *mxc* hypomorphic alleles encode nonsense mutations at residues K1482 and Q1643 of the 1837–amino acid long Mxc protein (White *et al.*, 2011). The resulting truncated mutant proteins support histone gene expression (Landais *et al.*, 2014), whereas an amorphic *mxc* allele that does not produce Mxc protein does not (White *et al.*, 2011). The Q1643 → Stop mutation ($mxc^{G46}$) partially disrupts Mxc function, resulting in replication stress and a persistent DNA damage response that contributes to the loss of germline stem cells through misregulation of histone gene expression (Landais *et al.*, 2014).

Studies in human cell culture indicate that distinct domains of NPAT are required to activate histone gene expression and allow entry into S phase (Wei *et al.*, 2003). These data suggest that Mxc/NPAT may contain multiple domains that organize HLB assembly and coordinate histone mRNA biosynthesis. Proteins harboring multiple protein–protein interaction domains are likely a critical feature of NBs (Matera *et al.*, 2009). The focal organization provided by the multiple interaction domains could facilitate a more efficient and rapid physiological response to distinct stimuli (Foray *et al.*, 2003; Zaidi *et al.*, 2007; Cortese *et al.*, 2008; Matera *et al.*, 2009; Good *et al.*, 2011; Bian *et al.*, 2012; Nussinov *et al.*, 2013). Here we identify functional domains of Mxc required for localization of Mxc to the HLB in the presence of full-length Mxc using cultured *Drosophila* S2 cells. We use *mxc*-mutant animals expressing different Mxc mutant transgenic proteins to explore the function of Mxc in vivo and time-lapse imaging of early embryos expressing GFP-Mxc to assess the dynamics of Mxc localization to the HLB. Our data indicate that Mxc requires multiple domains for complete function in vivo and that two self-interaction domains of Mxc are essential for HLB assembly, which in turn promotes histone mRNA biosynthesis.

## RESULTS

### Two $NH_2$-terminal domains are required for Mxc concentration in HLBs

The design of the Mxc mutants we analyzed for this study was directed by both homology to previously characterized protein domains and the properties of a collection of *mxc* mutant alleles (Santamaria and Randsholt, 1995) that we sequenced (White *et al.*, 2011). The 1837–amino acid Mxc protein contains only two small domains recognizable by primary sequence—a LisH domain at the N-terminus (amino acids 6–38) and a 13–amino acid–long AT-hook motif toward the C-terminus (amino acids 1523–1535). LisH domains are 33–amino acid motifs readily identifiable by primary sequence homology, with invariant hydrophobic residues at positions 9 and 13 and an aromatic residue at position 12 (Supplemental Figure S1A, arrowheads). Structural and biochemical analyses indicate that LisH domains adopt a characteristic fold that mediates protein–protein interactions, including homodimerization (Kim *et al.*, 2004; Cerna and Wilson, 2005; Gerlitz *et al.*, 2005; Mikolajka *et al.*, 2006). AT-hook domains bind the minor groove of DNA at AT-rich stretches and are characterized by an invariant peptide core motif of R-G-R-P that is well conserved and is flanked on both sides by positively charged amino acids (Reeves, 1990; Aravind, 1998; Harrer *et al.*, 2004). The $mxc^{G48}$-null allele, with AG-to-AA splice acceptor mutation at the intron 1/exon 2 border, does not produce detectable full-length Mxc protein. The three other alleles we sequenced ($mxc^{16a\text{-}1}$, $mxc^{G43}$, and $mxc^{G46}$) are predicted to generate altered Mxc proteins (Figure 1). The hypomorphic $mxc^{G43}$ and $mxc^{G46}$ alleles each has a mutation resulting in a premature stop codon and are predicted to express 1481– and 1642–amino acid long proteins, respectively. Although both of these alleles are viable, $mxc^{G43}$ has a stronger phenotype (consistent with having a larger deletion), with fewer progeny developing to adulthood than $mxc^{G46}$ (Santamaria and Randsholt, 1995). The $mxc^{16a\text{-}1}$ mutant contains a 4–base pair deletion/frameshift near the end of the open reading frame, resulting in replacement of the last 14 amino acids of Mxc with 45 residues not normally present in wild-type Mxc. Of interest, the $mxc^{16a\text{-}1}$ mutant is not viable, although it should produce an Mxc protein with a relatively small alteration at the C-terminus, compared with the more extensive deletions in $Mxc^{G43}$ and $Mxc^{G46}$.

To determine the regions of Mxc necessary for concentration in the HLB, we designed constructs encoding green fluorescent protein (GFP)–$Mxc^{16a\text{-}1}$, GFP-$Mxc^{G43}$, GFP-$Mxc^{G46}$, and three additional larger deletion mutants (GFP-$Mxc^{1\text{-}354}$, GFP-$Mxc^{1\text{-}721}$, GFP-$Mxc^{1\text{-}1172}$) as N-terminal GFP fusion proteins and expressed them in S2 cells (Figures 1 and 2). We stained transfected S2 cells with antibodies against GFP (to detect exogenous Mxc) and antibodies against FLASH or Mxc to mark the endogenous S2 cell HLB. Note that our

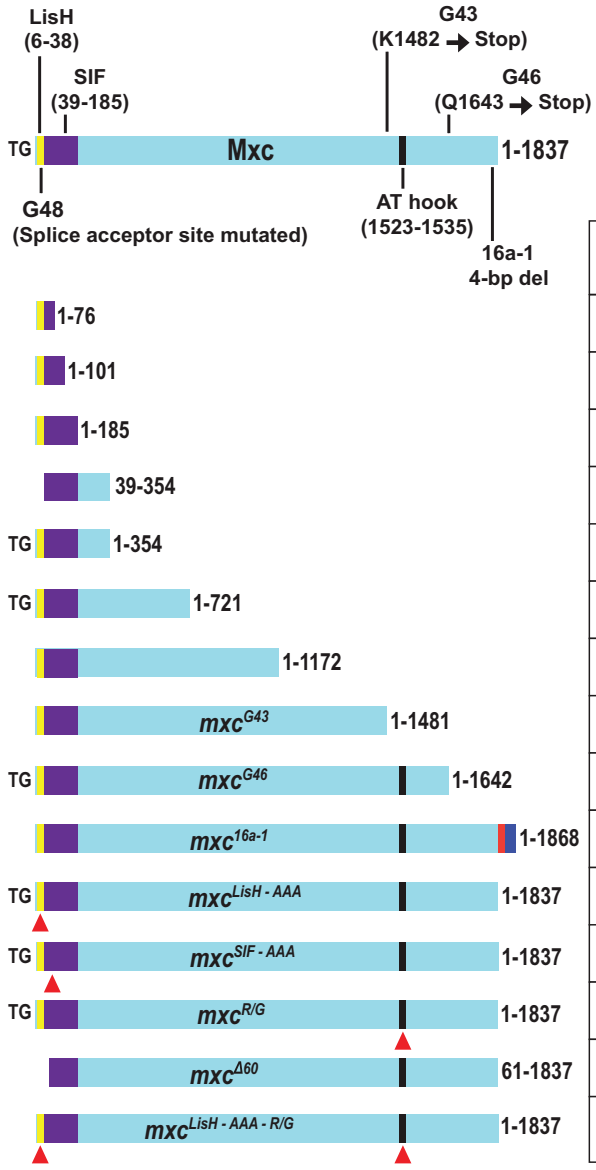


| Expressed protein | Mxc Accumulation in the HLB: wt Mxc present | wt Mxc absent |
|---|---|---|
| 1-76 | - | ND |
| 1-101 | + | ND |
| 1-185 | + | ND |
| 39-354 | - | ND |
| 1-354 | + | - |
| 1-721 | + | - |
| 1-1172 | + | ND |
| G43 | + | + |
| G46 | + | + |
| 16-a1 | + | - |
| LisH-AAA | ↓ | - |
| SIF-AAA | ↓ | - |
| R/G | + | + |
| Δ60 | - | ND |
| LisH-AAA R/G | - | ND |

FIGURE 1: Mxc structure/function analysis. Top, full-length Mxc displaying LisH (yellow), SIF (green), and AT-hook (black) domains and previously described mutations of *mxc*. Numbers to the left of each Mxc fragment indicate length in amino acids. Red arrowheads indicate V14, Y17, L18; L58, I61, I62; and R1528 point mutations in LisH, SIF, and AT-hook domains, respectively. TG, fragments used to generate transgenic flies. The table compiles results regarding the ability of each Mxc fragment to form a detectable HLB either in the presence or absence of wild-type (wt) Mxc. +, accumulation; –, no accumulation; ↓, decreased accumulation; ND, not determined.

Mxc antibody was raised against the last 169 amino acids of Mxc and therefore does not detect GFP-Mxc fusion proteins lacking the C-terminus of Mxc. The five deletion mutants, including the smallest, GFP-Mxc$^{1\text{-}354}$, were capable of concentrating in the endogenous HLB (Figure 2, A–G). The GFP-Mxc$^{16a\text{-}1}$ protein behaved differently from the deletion mutants: although we could detect some colocalization with FLASH in S2 cells, GFP-Mxc$^{16a\text{-}1}$ was also mislocalized in large foci throughout the nucleus. In addition, FLASH was also mislocalized in these cells (Figure 2H). This result indicates that the altered C-terminus encoded by *mxc*$^{16a\text{-}1}$ disrupts both Mxc and FLASH concentration in the HLB, an issue that we explore later.

We also tested whether the Mxc AT-hook domain was necessary for concentrating Mxc in the HLB in S2 cells. Mutation of the second conserved arginine of the Pro-Arg-Gly-Arg-Pro AT-hook consensus motif to glycine in high–mobility group protein A1a (HMGA1a) results in redistribution of HMGA1a within interphase nuclei (Harrer *et al.*, 2004). We therefore changed Arg$^{1528}$ of the Arg-Gly-Arg-Pro Mxc AT-hook motif to Gly (GFP-Mxc$^{R/G}$). GFP-Mxc$^{R/G}$ concentrated in the HLB in S2 cells similarly to control GFP-Mxc (Figure 2, B and I), suggesting that the AT-hook domain is not necessary to concentrate exogenous Mxc in the HLB, consistent with the results of the C-terminal deletion experiments that remove the AT-hook domain.

To define more precisely the sequences required for concentration in the HLB in S2 cells, we used N-terminal deletions to explore whether the LisH domain plays a role in concentrating Mxc in the HLB. We tested whether an otherwise full-length Mxc lacking the first 60 amino acids encompassing the LisH motif (GFP-Mxc$^{\Delta 60}$) would be able to concentrate in the HLB. GFP-Mxc$^{\Delta 60}$ did not concentrate in the HLB in S2 cells but instead was found throughout the nucleus (Figure 2J). A GFP-Mxc fragment lacking the LisH domain (GFP-Mxc$^{39\text{-}354}$) also failed to concentrate in the HLB (Figure 2K). These data suggest that the LisH domain is required for concentration of Mxc in the HLB. Note that endogenous FLASH also became partially mislocalized after expression of GFP-Mxc$^{\Delta 60}$ but not after expression of GFP-Mxc$^{39\text{-}354}$, which lacks the C-terminus (Figure 2, J and K). This result suggests that the presence of the C-terminus in a mislocalized Mxc can result in the mislocalization of FLASH, perhaps because the C-terminus of Mxc binds to FLASH.

Eleven of the first 12 amino acids in the LisH domain of Mxc are identical in all vertebrate NPATs, and overall the human NPAT LisH domain is 51% identical to that of Mxc. Three amino acids, Val-14, Tyr-17, and Leu-18, are conserved between the NPAT and Mxc LisH domains and well conserved among LisH domains in other proteins (Supplemental Figure S1A). Mutating these three amino acids to Ala, which is not expected to sterically hinder LisH-domain formation (Kim *et al.*, 2004), abrogated Mxc's concentration in the HLB in S2 cells (Figure 2L). GFP-Mxc$^{\text{LisH-AAA}}$ accumulated throughout the nucleus and caused some FLASH mislocalization, similar to GFP-Mxc$^{\Delta 60}$ (Figure 2, J and L). In addition, a GFP-Mxc$^{\text{LisH-AAA-R/G}}$ double mutant behaved similarly to the GFP-Mxc$^{\text{LisH-AAA}}$ single mutant (Figure 2M). Taken together, the LisH deletion and point mutant data indicate that the LisH domain plays an essential role in concentrating Mxc in the HLB. However, the LisH domain is not sufficient for HLB localization, as GFP-Mxc$^{1\text{-}76}$ did not concentrate in the HLB in S2 cells (Figure 2N). Together these data demonstrate that the LisH domain and residues between 76 and 354 of Mxc provide critical determinants for concentrating exogenous Mxc in the HLB in the presence of endogenous Mxc.

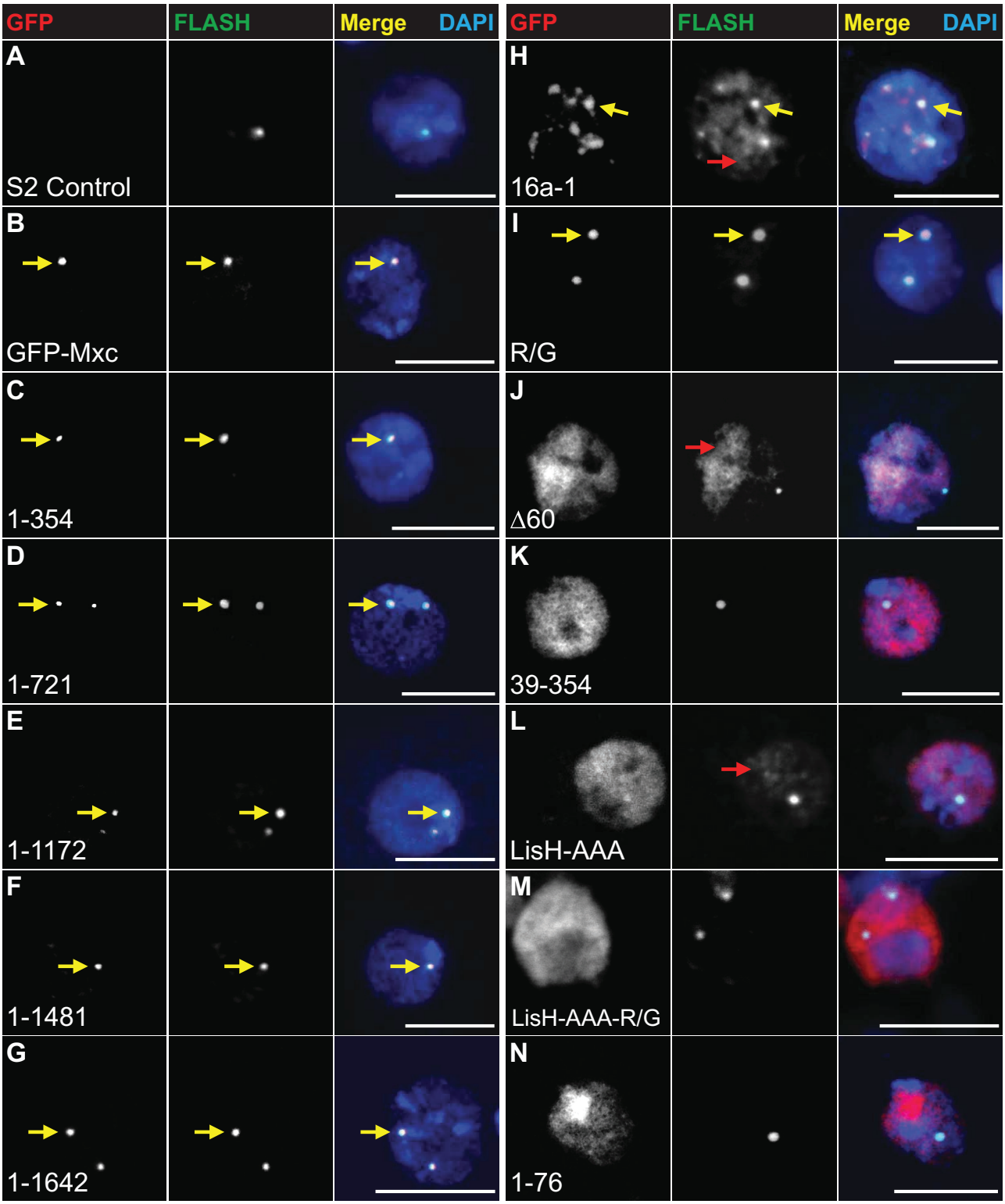


FIGURE 2: The Mxc N-terminus is required for concentration in the HLB in cultured cells. Untransfected S2 cells (A) or S2 cells transfected with constructs expressing the indicated GFP-Mxc proteins (B–N) were stained with anti-GFP and anti-FLASH antibodies. Yellow arrows indicate foci of colocalizing GFP-Mxc and FLASH. Note that transfection of mislocalized Mxc proteins with an intact C-terminus result in mislocalized FLASH (red arrows in H, J, and L). Bars, 10 μm.

### The Mxc N-terminus promotes Mxc self-interaction

Structural studies have shown that some LisH domains directly interact with each other, mediating dimerization (Kim *et al.*, 2004). We postulated that the N-terminal 354 amino acids of Mxc function to promote the self-interaction of Mxc molecules and that the LisH domain was part of this interaction. To explore this possibility, we conducted in vitro pull-down assays using a recombinant protein fragment expressed in *Escherichia coli* as maltose-binding protein (MPB)

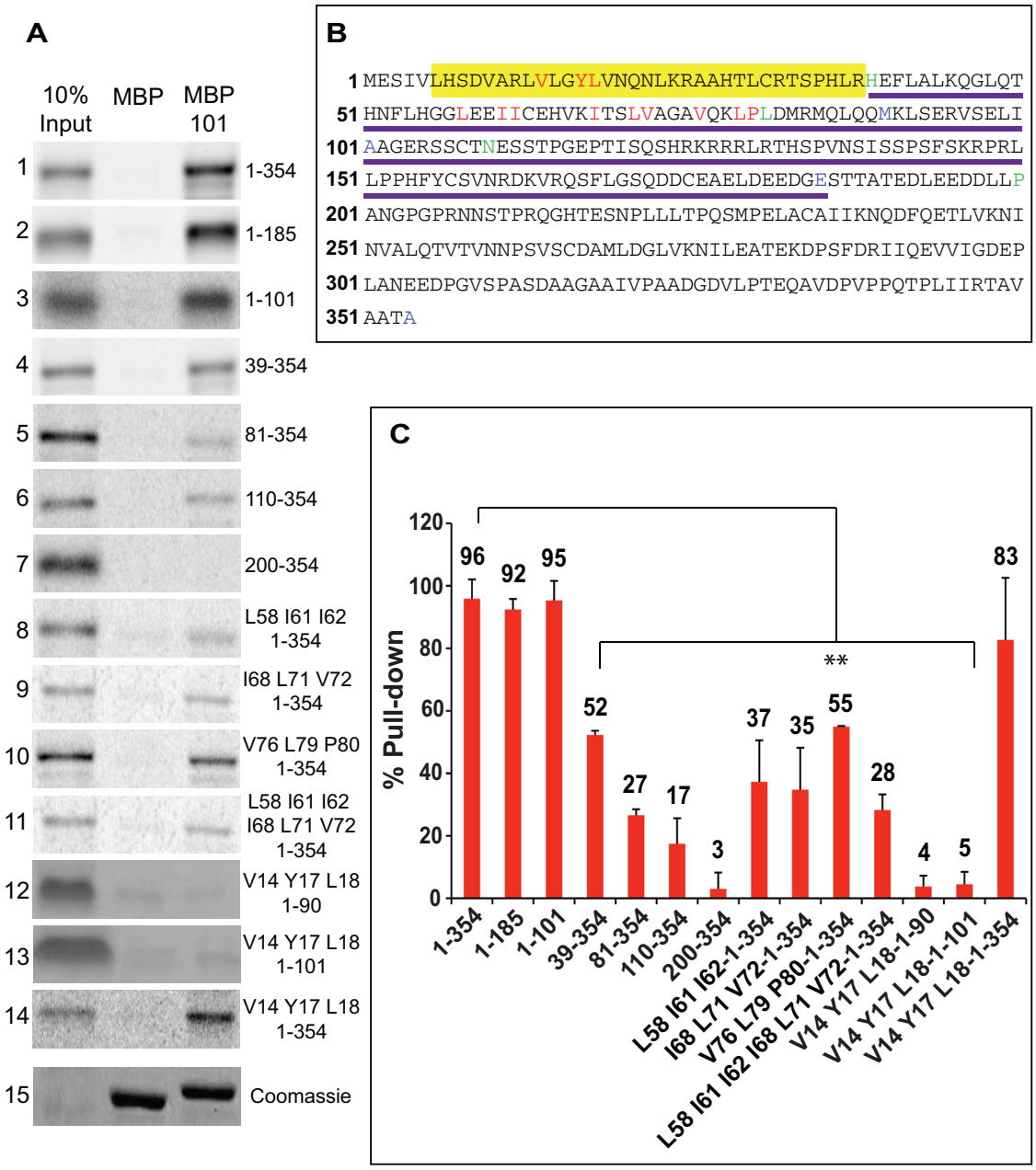


FIGURE 3: Mxc self-interaction requires two N-terminal domains. (A1–A14) $^{35}$S[Met]-labeled, in vitro–translated Mxc fragments (indicated at right) precipitated with MBP-Mxc$^{101}$ (MBP 101) and run side by side with 10% input to compare percentage of pull down. (A15) Coomassie-stained gel showing similar loading of recombinant MBP proteins. (B) Sequence of first 354 amino acids of Mxc with the LisH domain (L6-R38) indicated in yellow and the SIF domain (H39-E185) underlined. Amino acids in red indicate Ala substitution mutations in LisH (V14, Y17, and L18) and SIF (L58, I61, I62, I68, L71, V72, V76, L79, and P80) domains. Residues in green indicate N-terminal amino acids in the 39–354 (L39), 81–354 (L81), 110–354 (N110), and 200–354 (P200) fragments. Residues in blue indicate C-terminal amino acid in the 1–90 (M90), 1–101 (A101), 1–185 (E185), and 1–354 (A354) fragments. (C) Bar graph showing percentage of pull down for each Mxc fragment. Error bars represent SEM. The double asterisk indicates all statistically significant ($p < 0.001$) differences in binding compared with Mxc$^{1-354}$.

fused to the first 101 amino acids of Mxc (MBP-Mxc$^{101}$; Figure 3, A-15 and B). We expressed [$^{35}$S]methionine ([$^{35}$S]Met)-labeled Mxc fragments by in vitro translation in rabbit reticulocyte lysates and tested their ability to interact with recombinant MBP-Mxc$^{101}$. We efficiently pulled down [$^{35}$S]Met–labeled Mxc$^{1-354}$ using MBP-Mxc$^{101}$ but not with MBP alone, indicating that the N-terminus of Mxc interacts with itself (Figure 3A-1). Two shorter fragments of Mxc—Mxc$^{1-185}$ and Mxc$^{1-101}$—were also pulled down by MBP-Mxc$^{101}$ (Figure 3A-2 and -3) and were capable of concentrating in the S2 cell HLB as effectively as Mxc$^{1-354}$ (Supplemental Figure S3, A and B). Of interest, an Mxc fragment lacking the LisH domain (Mxc$^{39-354}$) was also pulled down by MBP-Mxc$^{101}$, indicating that Mxc self-interaction does not require LisH-domain homodimerization. The Mxc$^{39-354}$ was pulled down about half as efficiently as Mxc$^{1-354}$, Mxc$^{1-185}$, and Mxc$^{1-101}$ (Figure 3, A1–A4 and C). These results suggest that sequences in addition to the LisH domain can promote Mxc self-interaction.

Indeed, further deletion of the N-terminus ($Mxc^{81-354}$ and $Mxc^{110-354}$) further reduced, but did not abolish, binding to MBP-$Mxc^{101}$ (Figure 3, A-5 and -6 and C). A fragment from amino acid 200 to 354 ($Mxc^{200-354}$) did not bind MBP-$Mxc^{101}$ (Figure 3, A-7 and C). Taken together, these data suggest that residues downstream of the LisH domain between amino acids 39 and 101 are necessary for high-affinity Mxc self-interaction.

To identify candidate residues in this region, we performed an in silico structural analysis. LisH domains consist of a helix-turn-helix motif that typically homodimerizes. A homodimer of the Mxc LisH domain was modeled based on the crystallographic homodimer of the LisH domain of TBL1X (Protein Data Bank ID 2XTC). Analysis of the modeled Mxc homodimer revealed the possibility of a steric clash between His-7 of one LisH domain and Tyr-17 of the second LisH domain, suggesting that Mxc LisH domains do not homodimerize, consistent with our pull-down data. We hypothesized that additional structural motifs within the N-terminal 101 amino acids of Mxc would interact with the LisH domain and also contain residues in a similar helical structure that correspond to the highly conserved VxxYL hydrophobic residues within LisH domains that typically drive LisH homodimerization. We identified three sets of hydrophobic residues between amino acids 58 and 80 of Mxc that were in helical regions and might drive self-interaction. These three motifs were LxxII (L58-I61-I62), IxxLV (I68-L71-V72), and VxxLP (V76-L79-P80; Figure 3B). We therefore constructed three different sets of triple-Ala-substitution mutations in $Mxc^{1-354}$ and measured binding to MBP-$Mxc^{101}$ using the pull-down assay. The binding of $Mxc^{1-354}$ fragments containing L58A-I61A-I62A, I68A-L71A-V72A, or V76A-L79A-P80A mutation to MBP-$Mxc^{101}$ was reduced 50–65% relative to wild-type $Mxc^{1-354}$ (Figure 3, A-8–A-10, B, and C). An $Mxc^{1-354}$ fragment carrying both L58A-I61A-I62A and I68A-L71A-V72A mutations did not further reduce binding to MBP-$Mxc^{101}$ (Figure 3A-11). These data indicate that specific residues between amino acids 58 and 80 are required for efficient Mxc self-interaction, perhaps through a heterologous interaction with the LisH domain (Supplemental Figure S1B).

To interrogate further the role of the LisH domain in Mxc self-interaction, we generated $Mxc^{1-90}$ and $Mxc^{1-101}$ fragments containing the LisH triple-Ala mutation (V14A-Y17A-L18A; Supplemental Figure S1A). Either fragment harboring a mutagenized LisH domain showed >90% reduction in binding to MBP-$Mxc^{101}$ (Figure 3, A-12 and -13 and C). In contrast, the LisH-domain mutation in $Mxc^{1-354}$ did not significantly affect binding to MBP-$Mxc^{101}$ (Figure 3, A-14 and C). These data indicate that a mutant LisH domain has little affect on Mxc self-interaction when additional downstream residues are present. Because $Mxc^{200-354}$ does not bind MBP-$Mxc^{101}$ whereas $Mxc^{1-185}$ binds very well, we conclude that the C-terminal boundary of these additional amino acids is before residue 185. When all of our biochemical data are considered together (Figure 1), the results indicate that high-affinity Mxc self-interaction requires two distinct regions, the LisH domain (residues 6–38) and sequences between amino acids 39 and 185, which we designated the Mxc self-interaction facilitator (SIF) domain.

### Multiple Mxc domains including the N-terminal self-interaction domains are required for HLB formation in vivo and completion of development

To identify domains of Mxc required for in vivo function, we determined which of our Mxc transgenes (Figure 1) encoded proteins that concentrate in the HLB and whether they were capable of rescuing the lethality of the $mxc^{G48}$-null allele. These transgenes use the *ubiquitin-63E* promoter to ubiquitously express proteins with GFP fused to the N-terminus of wild-type or mutant Mxc. We first determined whether these proteins were present in the HLB in the presence of endogenous Mxc (Figure 4). GFP-Mxc concentrated in the HLB in embryos and ovarian follicle cells in the presence of the endogenous Mxc, as did the transgenic GFP-$Mxc^{1-354}$ and GFP-$Mxc^{1-721}$ proteins (Figure 4, A–D and G–J). In contrast, transgenic full-length $Mxc^{LisH-AAA}$ or $Mxc^{SIF-AAA}$ protein did not localize to the HLB in the presence of endogenous Mxc (Figure 4, E, F, K, and L).

Embryos that are homozygous for $mxc^{G48}$ hatch, develop to second-instar larvae, and then die. Expressing full-length GFP-Mxc in the homozygous $mxc^{G48}$ background completely rescued $mxc^{G48}$ lethality (i.e., supported development to adulthood) and resulted in assembly of HLBs that were indistinguishable from wild type (Supplemental Figure S2A). In fact, we can maintain a stock containing GFP-Mxc as the only functional copy of Mxc. GFP-$Mxc^{R/G}$, which contains a point mutation in the A/T- hook domain, is also capable of rescuing $mxc^{G48}$. In contrast, full-length Mxc harboring either a mutant LisH domain ($Mxc^{LisH-AAA}$) or a mutant SIF domain ($Mxc^{SIF-AAA}$) could not rescue $mxc^{G48}$ lethality or support HLB assembly (Supplemental Figure S2, B and C). The $Mxc^{SIF-AAA}$ allele contains the L58A-I61A-I62A mutation, which reduces self-interaction in the pull-down assay (Figure 3, A-8 and C), and we selected this mutation to test in vivo because these residues are conserved in human NPAT (Supplemental Figure S1C). Western blotting revealed that the $Mxc^{LisH-AAA}$ and $Mxc^{SIF-AAA}$ mutant proteins accumulate to levels similar to wild-type GFP-Mxc (Supplemental Figure S3C). These data indicate that the self-interaction domains we identified in vitro are required for Mxc function in vivo.

The GFP-$Mxc^{1-354}$ and GFP-$Mxc^{1-721}$ deletion mutants, which contain wild-type LisH and SIF domains and localized to the HLB in S2 cells and wild-type embryos and follicle cells, failed to rescue lethality of $mxc^{G48}$ or to support HLB assembly in the absence of endogenous Mxc (Supplemental Figure S2, B–E). This observation demonstrates that the concentration of GFP-$Mxc^{1-354}$ and of GFP-$Mxc^{1-721}$ in HLBs in S2 cells and wild-type embryos requires interaction with endogenous, full-length Mxc. Moreover, these results demonstrate that sequences between amino acid 721 and the C-terminus of Mxc are necessary for HLB assembly and *Drosophila* development.

To explore in more detail the functional domains within the 721–1837 region, we analyzed the hypomorphic mutants $mxc^{G46}$ and $mxc^{G43}$, which express Mxc proteins truncated at amino acids 1642 and 1481, respectively (Figure 1). Because our anti-Mxc antibody was raised against the last 169 amino acids of Mxc, it will not detect these proteins. We therefore generated a transgenic GFP-$Mxc^{G46}$ protein to determine whether this Mxc truncation is able to concentrate in the HLB. In a wild-type background, GFP-$Mxc^{G46}$ protein colocalizes at the histone locus with endogenous Mxc and FLASH (Figure 5A). In an $mxc^{G48}$-null background, GFP-$Mxc^{G46}$ forms foci resembling HLBs and rescues $mxc^{G48}$ lethality (Figure 5, B–E). In addition, $mxc^{G48}$ males expressing GFP-$Mxc^{G46}$ are sterile. Nuclear foci were detected in brains from $mxc^{G46}$ third-instar larvae or from $mxc^{G48}$ larvae expressing GFP-$Mxc^{G46}$ after staining with MPM-2, a monoclonal antibody that recognizes cyclin E/Cdk2–dependent phosphorylation sites in Mxc (Figure 5, F–H). Similarly, we detected MPM-2 foci in brains from $mxc^{G43}$-mutant larvae (Figure 5, I and J), which express an Mxc protein truncated at amino acid 1481 (Figure 1). A small fraction of $mxc^{G43}$ mutants survive to adulthood (Santamaria and Randsholt, 1995; Saget *et al.*, 1998; Remillieux-Leschelle *et al.*, 2002). Together these results demonstrate that a mutant Mxc with a C-terminal truncation to amino acid 1481 is capable of assembling into an HLB and supporting the completion of development, although inefficiently.

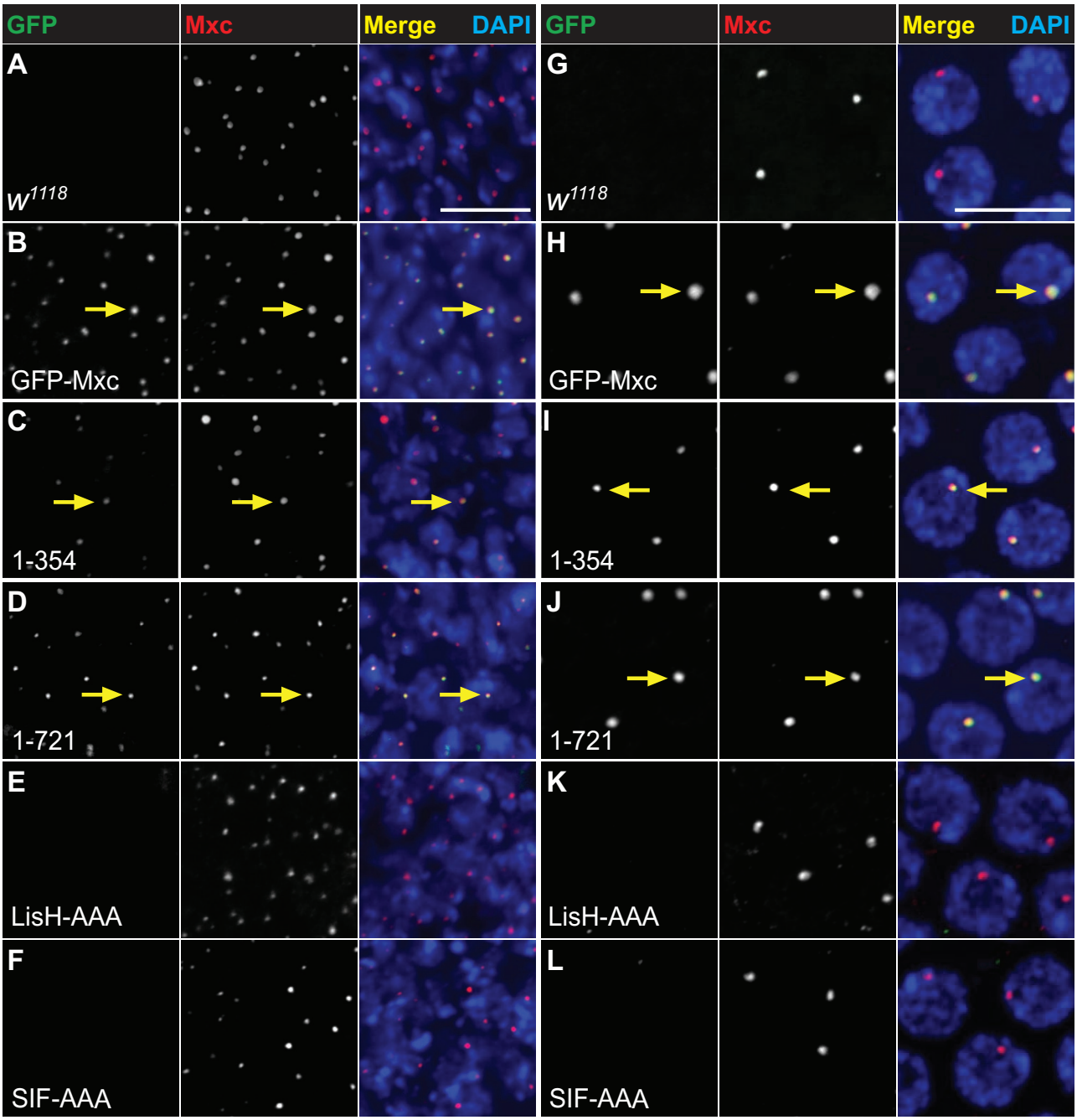


FIGURE 4: Mxc requires the LisH and SIF domains to concentrate at the histone locus in transgenic flies. We stained 8- to 10-h-old embryos (A–F) and ovarian follicle cells (G–L) expressing the indicated transgenes with anti-GFP and anti-Mxc antibodies. Note that GFP-Mxc$^{1\text{-}354}$ and GFP-Mxc$^{1\text{-}721}$ localize with endogenous Mxc (yellow arrows) but form smaller foci than GFP-Mxc. Bars, 10 µm (A–F), 5 µm (G–L).

### The C-terminus of Mxc recruits HLB components required for histone mRNA synthesis

To determine which domains of Mxc are necessary for histone mRNA transcription and pre-mRNA processing and the relationship between these processes and HLB formation, we measured total accumulation of histone H3 mRNA in our panel of mutants by fluorescence in situ hybridization (FISH) of 8- to 10-h-old embryos using a probe from the coding region of H3 (H3-cod). By 8 h of embryogenesis, the maternal stores of Mxc are substantially depleted as assayed by immunofluorescence (Figure 5C), as we previously reported (White *et al.*, 2011), allowing us to assess the capability of the different mutant GFP-Mxc proteins to support histone mRNA synthesis. In control embryos that have endogenous wild- type Mxc concentrated in the HLB, histone H3 mRNA accumulates in the cytoplasm of actively cycling cells (Figure 6A). In *mxc*$^{G48}$-null mutant embryos, histone H3 mRNA levels are reduced, and HLBs are not detectable with anti-Mxc antibodies that would only detect maternal Mxc (Figure 6B). Expression of GFP-Mxc restores HLB assembly and histone H3 mRNA expression (Figure 6C). GFP-Mxc$^{LisH\text{-}AAA}$ and GFP-Mxc$^{SIF\text{-}AAA}$ transgenic proteins in the *mxc*$^{G48}$-null background fail to concentrate in the HLB and fail to support normal accumulation of histone H3 mRNA (Figure 6, D and

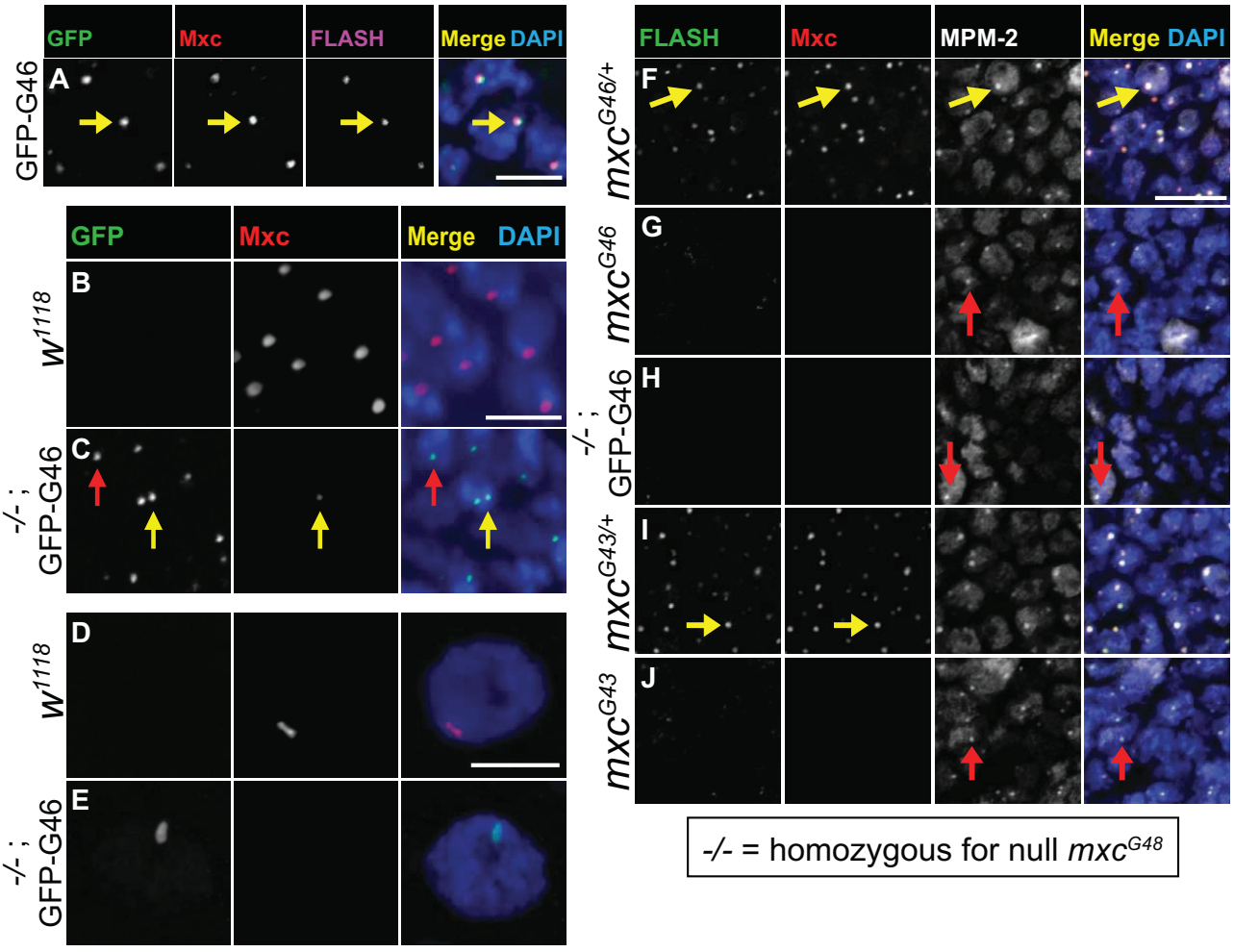


FIGURE 5: The 721–1481 region of Mxc is necessary for HLB assembly and completion of development. (A) An 8- to 10-h-old transgenic embryo expressing GFP-Mxc$^{G46}$ stained with anti- GFP, FLASH, and Mxc antibodies. Yellow arrow indicates GFP-Mxc$^{G46}$ localization to the endogenous HLB. (B, C) *w*$^{1118}$ control and a homozygous *mxc*$^{G48}$ mutant embryos expressing GFP-Mxc$^{G46}$ stained with anti- GFP and Mxc antibodies. The yellow arrow in C indicates a cell with an HLB containing a small amount of full-length, maternal Mxc still present (our anti-Mxc antibody does not recognize the truncated Mxc$^{G46}$ protein). The red arrow in C indicates a cell in which maternal Mxc has been depleted from the HLB. (D, E) Nuclei from salivary glands of *w*$^{1118}$ and *mxc*$^{G48}$*; gfp-G46* third-instar larvae stained with anti- GFP and Mxc antibodies. (F–J) Third-instar larval brains of the indicated genotypes stained with anti-FLASH, anti-Mxc, and MPM-2 antibodies. Yellow arrows indicate foci containing all three HLB markers. Red arrows indicate MPM-2–positive foci containing Mxc$^{G46}$, GFP-Mxc$^{G46}$, and Mxc$^{G43}$ (G, H, and J, respectively). Note that MPM-2 also detects other proteins in the nucleus. Bar, 5 μm (A–C), 10 μm (D–J).

E). We observed a similar phenotype with GFP-Mxc$^{1\text{-}354}$ and GFP-Mxc$^{1\text{-}721}$ (Figure 6, F and G), indicating that either mutation of the Mxc self-interaction domains or C-terminal truncation to amino acid 721 eliminates the ability of Mxc to support HLB formation and normal histone gene expression. In contrast, we detected slightly higher accumulation of histone H3 mRNA in the viable, hypomorphic truncation alleles *mxc*$^{G43}$ (residues 1–1481) and *mxc*$^{G46}$ (residues 1–1642; Figure 6, A, C, H, and I).

The in situ hybridization results were corroborated by Northern blot analysis of RNA extracted from 15- to 18-h-old embryos or early second-instar larvae near the lethal phase of the *mxc*$^{G48}$-null allele (Figure 6, K and L, respectively). Quantification of these data reveal a reproducible ~25% reduction of H3 mRNA accumulation in *mxc*$^{G48}$ relative to control embryos and that the GFP-Mxc$^{LisH\text{-}AAA}$, GFP-Mxc$^{SIF\text{-}AAA}$, GFP-Mxc$^{1\text{-}354}$, and GFP-Mxc$^{1\text{-}721}$ alleles are indistinguishable from null (Supplemental Figure S4). These data suggest that very small amounts of maternal Mxc in the HLB that is undetectable by immunofluorescence can support some histone mRNA expression or that there is a basal level of expression that can occur in the absence of Mxc. H3 mRNA accumulation in *mxc*$^{G43}$ and *mxc*$^{G46}$ embryos is reduced relative to control but less so than the null alleles. Curiously, in the *mxc*$^{G43}$ and *mxc*$^{G46}$ larval samples, H3 mRNA accumulation is greater than in control, consistent with a previous study (Landais *et al.*, 2014). The mechanistic basis for the *mxc*$^{G43}$ and *mxc*$^{G46}$ H3 larval mRNA expression phenotype is not known.

We next determined whether histone pre-mRNA processing was disrupted in our panel of Mxc mutants. Loss of histone pre-mRNA processing factors, such as the stem loop binding protein (SLBP) or U7 snRNP, results in transcription past the normal processing site, use of cryptic, downstream polyadenylation signals, and accumulation of cytoplasmic poly A+ histone mRNA (Sullivan *et al.*, 2001; Godfrey *et al.*, 2006). These aberrant histone H3 transcripts are readily detected by in situ hybridization using a probe (H3-ds) derived from sequences downstream of the normal H3 mRNA 3′ end

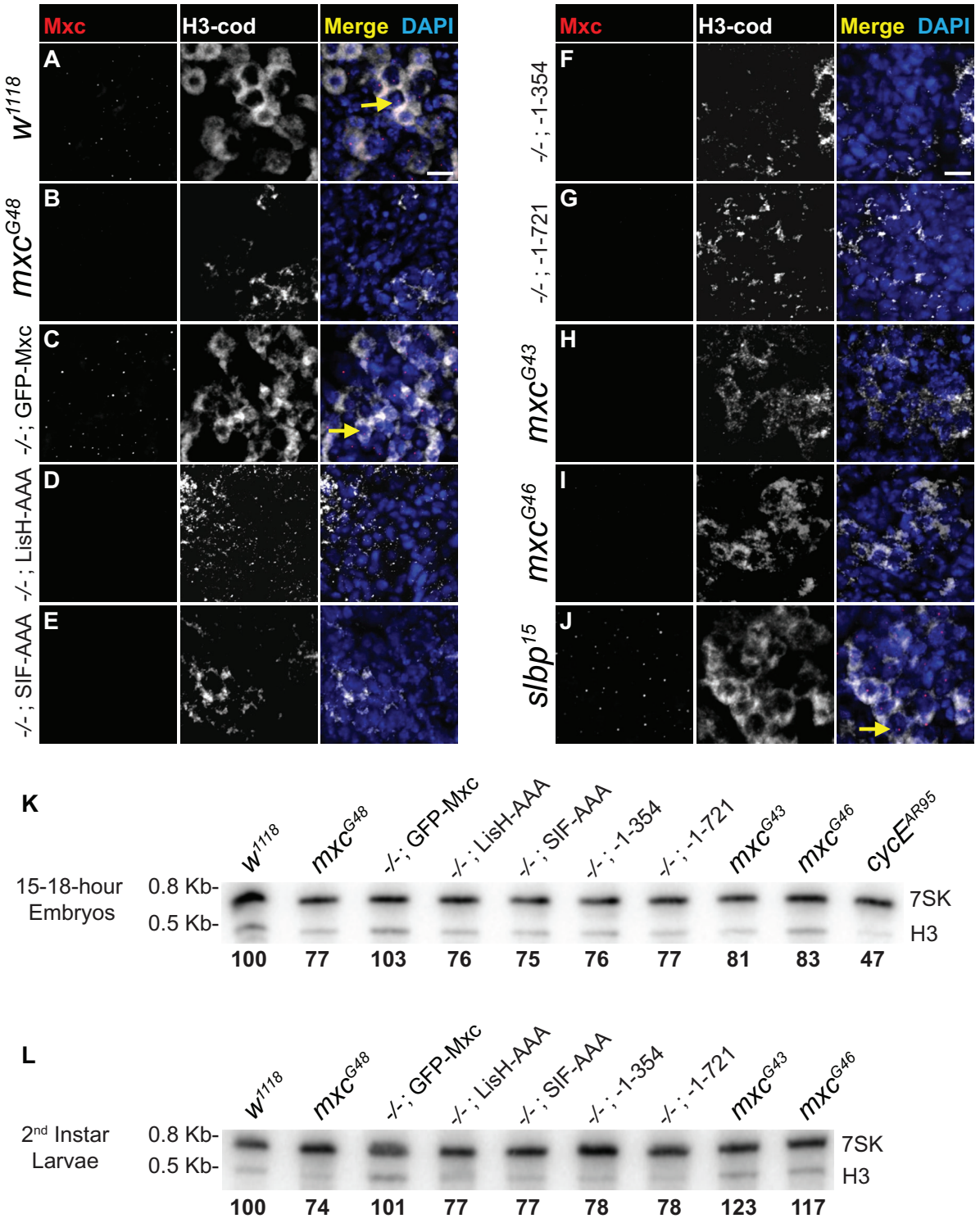


FIGURE 6: Mxc concentration in the HLB is required for histone mRNA biosynthesis. (A–J) We subjected 8- to 10-h-old embryos of the indicated genotypes to FISH with an RNA probe generated from the H3-coding region (H3-cod) and costained with anti-Mxc antibodies. Images of epithelial cells were specifically obtained from the cephalic region. Yellow arrows indicate Mxc foci in the nuclei of actively cycling cells that accumulate histone H3 mRNA in the cytoplasm. Note that *mxc*$^{G43}$- and *mxc*$^{G46}$-mutant embryos (H, I) accumulate detectable amounts of H3 mRNA. Bars, 10 µm. (K, L) Northern blot analysis of histone H3 transcript levels from two developmental stages of different *mxc* mutants. A 1-µg amount of total RNA from 15- to 18-h-old embryos (K) and 5 µg of total RNA from second-instar larvae (L) per well were run on a 6% acrylamide 8 M urea denaturing gel. 7SK RNA was used as a loading control on both gels. Numbers below each lane represent the averaged percentage of histone H3 transcript levels obtained from three independent experiments. Homozygous *cycE*$^{AR95}$-mutant embryos were used as a control, as cyclin E is known to be required for DNA replication and cell cycle progression in dividing and endocycling cells after cycle 16 (Knoblich *et al.*, 1994) and also for histone mRNA expression (Lanzotti *et al.*, 2004a).

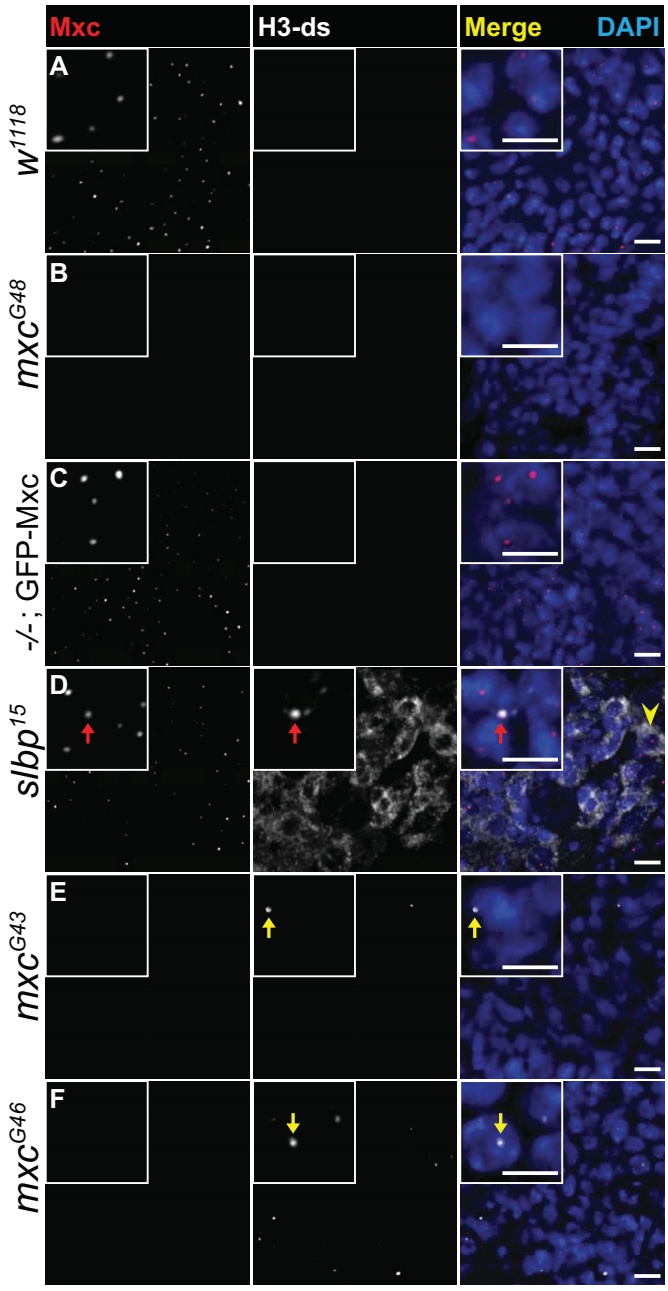


FIGURE 7: The C-terminus of Mxc is required to concentrate essential histone mRNA–processing factors at the histone locus. (A–F) The 8-to 10-h-old embryos of the indicated genotypes were subjected to FISH with an RNA probe generated from a region downstream of the normal H3 pre-mRNA processing site (H3-ds) and costained with anti-Mxc antibodies. Images were obtained of epithelial cells from the cephalic region. Insets show a higher magnification of nuclei. Red arrows in D indicate foci of nascent, unprocessed H3 RNA that colocalize with Mxc at the histone locus in *slbp*$^{15}$ homozygous mutant embryos (Lanzotti *et al.*, 2004a). Note that in *slbp*$^{15}$-mutant embryos, the H3 RNA is misprocessed to poly A+ mRNA, which is exported to and accumulates in the cytoplasm (yellow arrowhead in D). Yellow arrows in E and F indicate foci of nascent, unprocessed H3 RNA in nuclei of *mxc*$^{G43}$-mutant (E) and *mxc*$^{G46}$-mutant (F) embryos. Scale bars, 10 μm (A–F), 5 μm (insets).

(Lanzotti *et al.*, 2002, 2004a). The H3-ds probe does not hybridize to wild-type, *mxc*$^{G48}$-null mutant, *mxc*$^{G48}$, or GFP-Mxc–rescued embryos or the cytoplasm of *mxc*$^{G43}$ or *mxc*$^{G46}$ embryos because all of the histone mRNA is processed normally, as judged by Northern blotting (Figure 6, K and L), and the H3-ds probe does not detect processed H3 mRNA (Figure 7, A–C). In contrast, in *Slbp*$^{15}$-null mutant embryos, the H3-ds probe detects nascent, readthrough H3 transcripts in the nucleus that colocalize with Mxc-positive HLBs (Figure 7D, red arrow). These readthrough transcripts are processed to poly A+ H3 mRNA and exported to the cytoplasm, where they are detected with either the H3-cod (Figure 6J) or H3-ds probes (Figure 7D, yellow arrowhead; Lanzotti *et al.*, 2002, 2004b).

Using this assay, we determined whether any of the Mxc mutants accumulate unprocessed H3 mRNA at the site of transcription. As expected, the H3-ds probe did not hybridize to Mxc-mutant embryos with GFP-Mxc$^{LisH\text{-}AAA}$, GFP-Mxc$^{SIF\text{-}AAA}$, GFP-Mxc$^{1\text{-}354}$, and GFP-Mxc$^{1\text{-}721}$ transgenic proteins that failed to assemble an HLB and consequently failed to express H3 mRNA in the *mxc*$^{G48}$-null background (unpublished data). In contrast, we detected robust nuclear foci with the H3-ds probe in both *mxc*$^{G43}$- and *mxc*$^{G46}$-mutant embryos (Figure 7, E and F). *mxc*$^{G46}$ embryos reproducibly contained more and brighter H3-ds foci than homozygous *mxc*$^{G43}$ embryos (Figure 7, E and F), suggesting a higher rate of histone gene transcription in the *mxc*$^{G46}$ mutant (Figure 6, H, I, and K). In each mutant, the H3-ds foci were fewer and dimmer than in *Slbp*$^{15}$-mutant embryos (Figure 7, D–F), perhaps because wild-type Mxc and the normal HLB in the *Slbp*$^{15}$ mutants drives more transcription than the Mxc$^{G43}$- and Mxc$^{G46}$-mutant proteins.

The FLASH protein, which is essential for histone pre-mRNA processing, is not concentrated in the HLB in *mxc*$^{G43}$ and *mxc*$^{G46}$ mutants (Figure 5, G and J; Rajendra *et al.*, 2010), providing a possible explanation for the presence of misprocessed H3 mRNA. Of interest, using the H3-ds probe, we did not detect misprocessed H3 mRNA in the cytoplasm of *mxc*$^{G43}$- and *mxc*$^{G46}$-mutant cells, although we did detect histone mRNA with the H3-cod probe (Figure 6, H and I). This result suggests that the nascent readthrough transcripts are ultimately processed at the normal site and exported. We explore this observation in more depth in a separate study (D. Tatomer, E. A. Terzo, W. F. Marzluff, and R. J. Duronio, unpublished data).

### Both the LisH and SIF domains are required for efficient accumulation of Mxc in the HLB

Although the severe phenotypes observed with large C-terminal deletions of Mxc are not surprising, two different 3–amino acid changes (Mxc$^{LisH\text{-}AAA}$ and Mxc$^{SIF\text{-}AAA}$) effectively inactivated the 1837-residue Mxc protein. To investigate more carefully the effects that mutating the self-interaction domains has on Mxc localization and behavior in vivo, we conducted time-lapse imaging experiments on live embryos expressing GFP-Mxc$^{LisH\text{-}AAA}$ and GFP-Mxc$^{SIF\text{-}AAA}$. We focused on the first 2 h of embryogenesis, when HLB formation first occurs (White *et al.*, 2011). At this time, *Drosophila* embryos are a syncytium in which nuclei undergo 13 rapid, synchronous cycles composed only of S phase and mitosis (Swanhart *et al.*, 2005). With our previous imaging of fixed embryos, we first detected Mxc nuclear foci during cycle 10, one cycle before histone gene expression begins (White *et al.*, 2011). By imaging live embryos expressing GFP-Mxc and H2Av–red fluorescent protein (RFP) to visualize chromosomes, we detected small GFP-Mxc nuclear foci as early as interphase of cycle 9 (Figure 8, A and A′, and Figure 8 Supplemental Movie 1), suggesting that the live-imaging approach is more sensitive. These foci become larger in each subsequent cycle, as more-defined and much brighter GFP-Mxc foci become visible during interphase of cycle 10 and again in cycle 11,

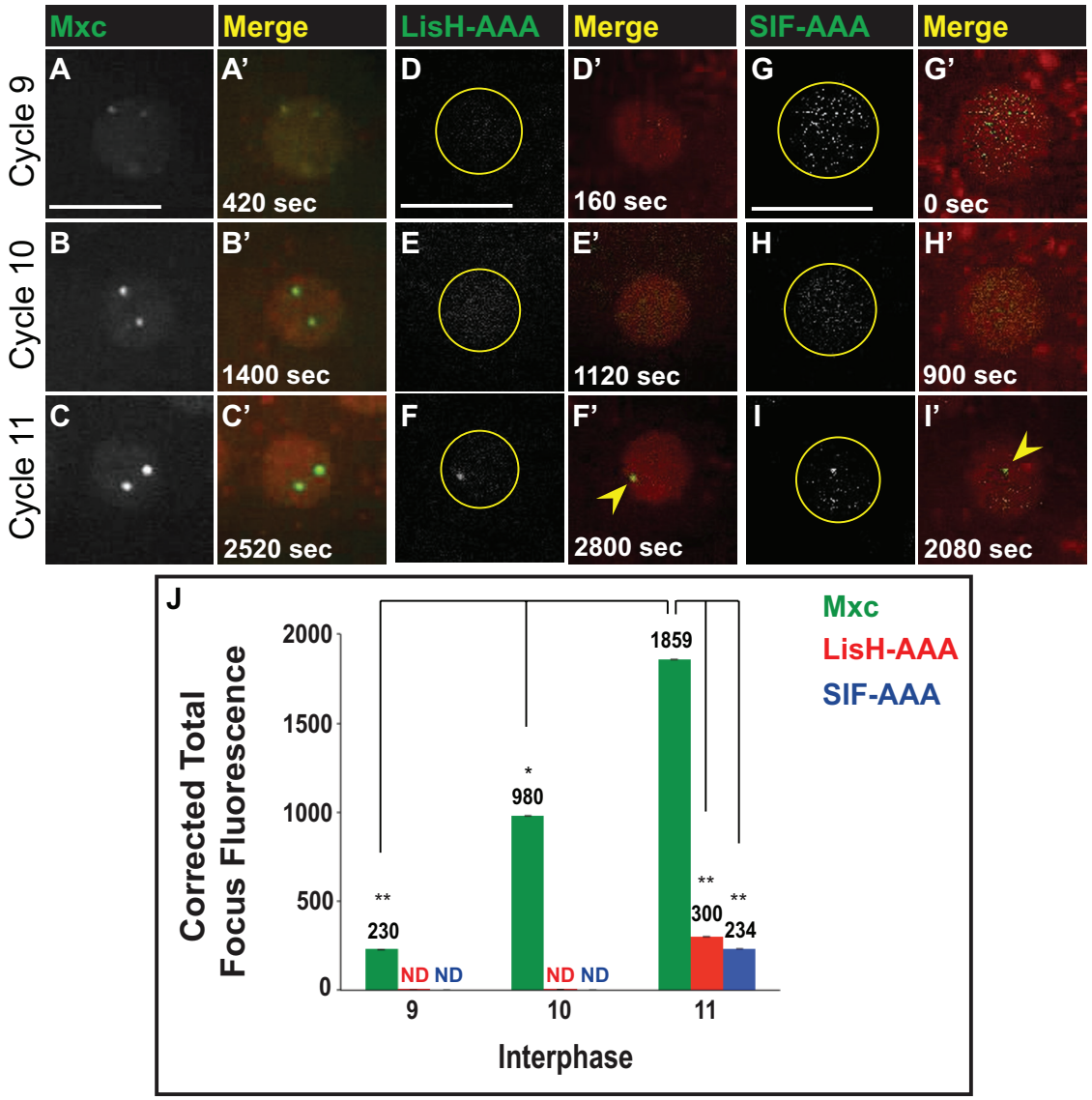


FIGURE 8: Mxc's LisH and SIF domains promote HLB localization. (A–I') Still images take from time-lapse movies of syncytial *H2Av-rfp/gfp-mxc*, *H2Av-rfp/gfp-mxc*$^{LisH\text{-}AAA}$, and *H2Av-rfp/gfp-mx*$^{SIF\text{-}AAA}$ transgenic embryos. Yellow circles denote the nuclear periphery. Yellow arrowheads point to dim foci of Mxc$^{LisH\text{-}AAA}$ (F') and Mxc$^{SIF\text{-}AAA}$ mutant proteins (I'). Note that red signal outside of nuclei are lipid droplets containing maternally supplied H2Av protein (Li *et al.*, 2014). Bars, 10 µm. (J) Bar graph showing corrected total focus fluorescence values from interphase of cycles 9–11. Error bars represent SEM. Numbers above bars represent averaged CTFF values. ND , not determined CTFF values due to undetectable foci. Significant differences are indicated either by a single ($p < 0.05$) or double ($p < 0.001$) asterisk.

when the mature HLB has formed (Figure 8, B, C, and J, and Figure 8 Supplemental Movie 1). In addition, we detected small GFP-Mxc foci associated with mitotic chromosomes (Supplemental Figure S5, A–A''), as we previously observed in fixed embryos (White *et al.*, 2011). Our live imaging also revealed a low level of GFP-Mxc signal coincident with the H2Av-RFP signal from condensed mitotic chromosomes (Supplemental Figure S5, B–B''). One possibility for this observation is that Mxc associates with all chromosomes during mitosis and then becomes concentrated in the HLB at the histone locus during interphase. However, we cannot eliminate the possibility that this chromosome interaction results from overexpression of GFP-Mxc relative to endogenous Mxc and does not normally happen.

The increase in intensity of GFP-Mxc foci during cycles 9–11 (Figure 8J) suggests that the HLB expands in size after initial nucleation or "seeding" as early as cycle 9. To test whether this HLB expansion requires Mxc self-interaction, we performed live-imaging experiments with GFP-Mxc$^{LisH\text{-}AAA}$ and GFP-Mxc$^{SIF\text{-}AAA}$. To our surprise, we observed discrete foci of GFP-Mxc$^{LisH\text{-}AAA}$ and GFP-Mxc$^{SIF\text{-}AAA}$, again suggesting that our live imaging is more sensitive than our imaging of fixed embryos. The GFP-Mxc$^{LisH\text{-}AAA}$ and GFP-Mxc$^{SIF\text{-}AAA}$ foci were considerably dimmer than those formed by GFP-Mxc and were first detectable in cycle 11 rather than cycle 9 (Figure 8, D–I' and J, and Figure 8 Supplemental Movies 2 and 3). These results indicate that Mxc$^{LisH\text{-}AAA}$ and GFP-Mxc$^{SIF\text{-}AAA}$ are defective for HLB accumulation during the syncytial cycles. Both mutant proteins also associated with mitotic chromosomes, but again these signals were weaker than that obtained with GFP-Mxc (Supplemental Figure S5, C–F''). Out of necessity, these experiments were performed in the presence of maternal supplies of wild-type Mxc; therefore the small

foci and mitotic chromosome association may result from a weak interaction between endogenous Mxc and either GFP-Mxc$^{LisH\text{-}AAA}$ or GFP-Mxc$^{SIF\text{-}AAA}$. These data indicate that GFP-Mxc$^{LisH\text{-}AAA}$ and GFP-Mxc$^{SIF\text{-}AAA}$ are defective in HLB localization and suggest that Mxc self-interaction is a critical component of HLB assembly during development.

## DISCUSSION

HLBs assemble at replication-dependent histone loci and provide a distinct compartment in the nucleus that promotes efficient transcription and processing of histone mRNA, likely by concentrating histone biosynthetic factors, as well as excluding factors specifically required for polyadenylation (Dundr, 2012). In this study, we show that multiple protein domains are necessary for Mxc to support HLB assembly and histone mRNA biosynthesis and ultimately normal *Drosophila* development.

### Multiple domains of Mxc are required for HLB assembly

Whether NBs form by an ordered assembly process, random association of components, or a combination of each of these processes is not clear for most NBs (Matera *et al.*, 2009). In the case of the HLB, we demonstrated that hierarchical assembly contributes to NB formation, with Mxc and FLASH part of a complex that initially forms at a specific sequence at the histone locus (White *et al.*, 2011; Salzler *et al.*, 2013). Here we defined two regions in the N-terminus of Mxc—the LisH domain and a novel domain we named the SIF domain—both of which are necessary for GFP-Mxc to concentrate in the HLB in the presence of endogenous Mxc and support HLB assembly in the absence of endogenous Mxc.

Although GFP-Mxc$^{1\text{-}354}$ and GFP-Mxc$^{1\text{-}721}$, which contain both LisH and SIF domains, are incorporated into the HLB in the presence of endogenous Mxc, they do not support formation of a complete HLB in the absence of endogenous Mxc and cannot rescue the lethality caused by an *mxc*-null mutation. Thus sequences in addition to the LisH and SIF domains are required for HLB formation. Truncated Mxc proteins encoded by the viable, hypomorphic *mxc*$^{G43}$ and *mxc*$^{G46}$ alleles (1481 and 1642 amino acids, respectively) form nuclear bodies (HLBs), as judged by staining tissues with the MPM-2 antibody, which recognizes phosphorylated Mxc, and formation of nuclear foci by GFP-Mxc$^{G46}$ protein in the absence of endogenous Mxc. Thus there is a region of Mxc between amino acids 721 and 1481 that together with the N-terminus is required for HLB formation. The larger Mxc proteins likely contain elements necessary for recruitment of Mxc to the H3-H4 intergenic region of the histone locus that is essential for HLB formation (Salzler *et al.*, 2013). However, because maternal supplies of wild-type Mxc initially establish the HLB in the early embryo before the zygotic expression of *mxc*$^{G43}$ and *mxc*$^{G46}$, we cannot be certain that Mxc$^{G43}$ and Mxc$^{G46}$ proteins are capable of forming an HLB de novo. Finally, Mxc likely contains binding sites for other HLB components, such as FLASH, U7 snRNP, or Mute, and is regulated by phosphorylation by cyclin E/Cdk2.

### Self-interaction between different Mxc molecules is required for HLB assembly

LisH domains are found in a variety of multiprotein complexes and promote protein–protein interactions important for the assembly of these complexes (Kim *et al.*, 2004; Cerna and Wilson, 2005; Gerlitz *et al.*, 2005; Mikolajka *et al.*, 2006). Some LisH-domain proteins dimerize through their LisH domains, and a structure of a LisH-domain homodimer has been solved (Kim *et al.*, 2004). We find that the Mxc N-terminus promotes interaction of two Mxc molecules but that this interaction does not occur by LisH-domain homodimerization. In Mxc, there is a possible steric clash between His-7 of one LisH domain and Tyr-17 of a second LisH domain, which may explain why the Mxc LisH domains do not homodimerize in a manner typical of other LisH domains. Instead, Mxc self-interaction requires a region downstream of the LisH domain between amino acids 39 and 185 (the SIF domain), and three amino acids (Leu-52, Ile-61, and Ile-62) in this region conserved between flies and vertebrates are required for HLB assembly in vivo and for rescuing the lethality of an *mxc*-null mutation. Furthermore, live imaging revealed dramatically reduced concentration of GFP-Mxc$^{LisH\text{-}AAA}$ and GFP-Mxc$^{SIF\text{-}AAA}$ in HLBs in the presence of endogenous Mxc, consistent with reduced binding affinity between the mutant and wild-type Mxc molecules.

Thus the LisH domain of one molecule of Mxc binds the SIF domain (i.e., amino acids 39–185) of another molecule of Mxc. Our molecular modeling suggests that this interaction may be mediated by direct binding between the LisH domain and the LxxII motif of the SIF domain (Figure 9). In addition to the LxxII motif, the SIF domain contains other amino acids that contribute to efficient Mxc self-interaction. These multiple interaction sites indicate that each Mxc molecule can potentially interact with at least two and possibly more Mxc molecules, raising the possibility that the N-terminal region of Mxc can promote formation of a three-dimensional lattice that is likely an essential component of HLB structure (Figure 10). Similarly, an N-terminal domain of coilin that mediates self-interaction is necessary for coilin accumulation in the Cajal body (Hebert and Matera, 2000), suggesting that oligomerization is a common feature of NB formation.

Many LisH domain–containing proteins also contain a CTLH domain (C-terminus to LisH), defined in both ProSite and SMART (Emes and Ponting, 2001; Adams, 2002; Umeda *et al.*, 2003), which is often but not always immediately C-terminal to the LisH domain. Other than the prediction that this domain contains α-helical regions, there is no structural information on the CTLH domain. The CTLH domains of several proteins have been shown to participate in protein–protein interactions important for the assembly of multiprotein complexes (Kobayashi *et al.*, 2007; Menssen *et al.*, 2012; Sun *et al.*, 2013;

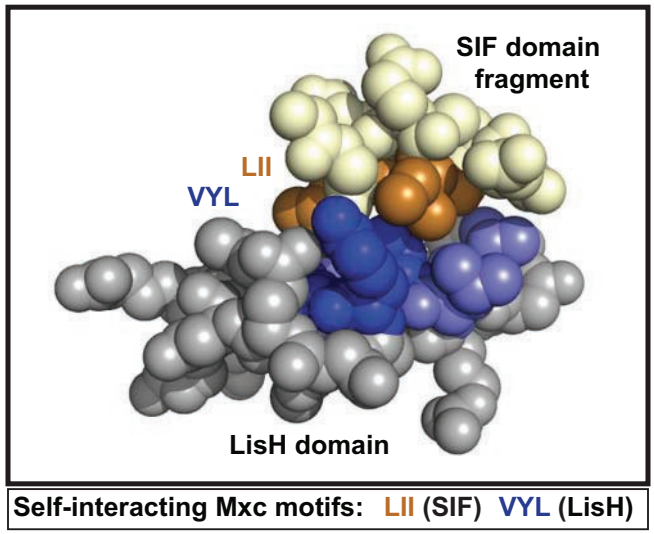


FIGURE 9: LisH-domain/SIF-domain self-interaction model. Space-filling model of the proposed interaction of the Mxc LisH domain with the Mxc SIF domain. The LisH domain of Mxc is light gray, with the VYL motif colored dark blue and neighboring hydrophobic residues in LisH colored slate blue. A small fragment of the SIF domain (GGLEEIICE) rendered in PyMOL is colored light yellow, with the critical LII motif colored copper.

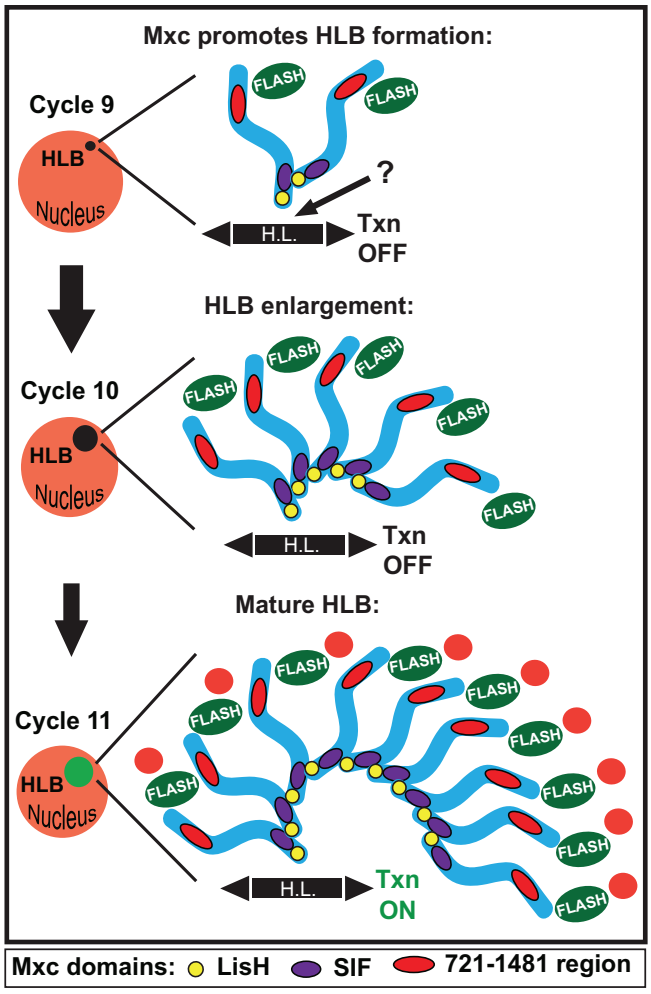


FIGURE 10: HLB assembly model. Mxc along, with FLASH, first associates with the histone locus (H.L.), but if and how Mxc binds DNA directly or through a DNA-binding protein remains unknown (?). Once chromosome associated, Mxc initiates the formation of a three-dimensional HLB lattice by accumulating more Mxc molecules from the nucleoplasm via a LisH domain (yellow circle)/SIF domain (purple oval)–dependent self-interaction as early as syncytial nuclear cycle 9. During cycle 10, when histone transcription has not yet begun (black nuclear circle), approximately fourfold enlargement of the HLB lattice is observed, which requires Mxc's N-terminus (LisH and SIF domains) and a region between amino acids 721 and 1481 (red oval). During cycle 11, when zygotic histone gene expression begins (green nuclear circle), the HLB lattice further increases its size, and other histone mRNA biosynthetic factors are recruited to the HLB (orange circles). In addition to a structural role, Mxc may also contribute to HLB formation by directly binding DNA and stimulating histone gene transcription (Salzler *et al.*, 2013).

Salemi *et al.*, 2014). The Mxc SIF domain that we identified functions similarly to the CTLH domain, but is clearly distinct from it. The SMART and ProSite CTLH-domain logos each contains a conserved glycine (G) at position 16, a conserved phenylalanine (F) at position 46, a conserved leucine (L) at position 48, and a conserved glutamic acid (E) at position 55 (numbering of SMART logo), none of which is present in the SIF domain of Mxc. Thus the region in Mxc C-terminal to the LisH domain is distinct from the CTLH domain.

Harper and colleagues demonstrated that human NPAT is essential for cell proliferation and histone gene expression and that the NPAT LisH domain is necessary for stimulating His4 and H2B promoter activation in cell culture–based transfection/reporter assays (Wei *et al.*, 2003; Ye *et al.*, 2003). They also reported that a LisH domain–mutant NPAT protein could localize to coilin-positive NBs (a subset of which are likely to be HLBs; Wei *et al.*, 2003). However, these experiments were performed by transfecting RAT1 cells containing endogenous NPAT, and the role of the LisH domain in NB formation, cell proliferation, and histone gene expression was not examined in the absence of endogenous NPAT. In addition, mutations of the NPAT SIF domain were not generated and analyzed in these previous studies. On the basis of our results and the similarity between the N-termini of mammalian NPAT and Mxc (Supplemental Figure S1), we suspect that human NPAT LisH-domain mutants can interact with endogenous NPAT via the SIF and/or other domains. We propose that the N-terminus of human NPAT promotes interaction between multiple NPAT molecules.

### Mxc's requirement for histone mRNA biosynthesis correlates with HLB assembly

Our prior imaging of fixed embryos and our live imaging reported here indicate that maternal Mxc and FLASH colocalize in nuclear foci before the initiation of zygotic histone gene transcription in the syncytial embryo (White *et al.*, 2007, 2011; Salzler *et al.*, 2013). Once histone transcription initiates, these foci enlarge into mature HLBs, as detected by increased intensity of both Mxc and FLASH staining, as well as by recruitment of other HLB components, U7 snRNP and Mute. We previously reported that *mxc* null–mutant first-instar larvae fail to accumulate normal amounts of histone H3 mRNA, supporting a role for Mxc in histone gene expression (White *et al.*, 2011). Here we show that the maternal supply of Mxc (as determined by detection of HLBs by immunofluorescence) is depleted in most cells by 8 h of embryogenesis and that this depletion is accompanied by a decrease in histone H3 transcript levels. In spite of reduced levels of histone mRNA, *mxc* null–mutant embryos hatch. Thus, as the maternal supply of Mxc is depleted in *mxc*-mutant embryos, histone gene expression drops, resulting in death in early larval stages.

In contrast to the null allele, hypomorphic *mxc*-mutant embryos ($mxc^{G43}$ and $mxc^{G46}$) develop to adults and hence are capable of supporting histone mRNA biosynthesis, consistent with previous observations (Landais *et al.*, 2014). In ovaries, the 1642–amino acid $Mxc^{G46}$ protein fails to recruit FLASH to HLBs (Rajendra *et al.*, 2010) and results in accumulation of small amounts of misprocessed histone H3 mRNA (D. Tatomer, E. A. Terzo, W. F. Marzluff, and R. J. Duronio, unpublished data). Here we report that unprocessed histone H3 RNA accumulates at the histone locus in $mxc^{G43}$-and $mxc^{G46}$-mutant embryos. This nascent, unprocessed H3 RNA was detected by in situ hybridization with a probe derived from sequence downstream of the normal H3 mRNA 3′ end. We do not detect these unprocessed RNAs in wild-type embryos. Thus loss of the last 195 amino acids from Mxc may reduce the efficiency of normal histone mRNA 3′ end formation.

### Conclusions

Several lines of evidence suggest that proteins with multiple protein–protein interaction domains mediate the localized concentration of components that give rise to NBs (Foray *et al.*, 2003; Zaidi *et al.*, 2007; Matera *et al.*, 2009; Good *et al.*, 2011). NB components can exchange with the nucleoplasm (Deryusheva and Gall, 2004; Dundr *et al.*, 2004), suggesting that there are multiple relatively weak protein–protein interactions between components of nuclear bodies, a property that is shared with other cellular bodies (e.g., P-bodies and stress granules in the cytoplasm;

Dundr and Misteli, 2010; Voronina *et al.*, 2011). In connection with this and our previous work (White *et al.*, 2011; Salzler *et al.*, 2013), we propose a model in which Mxc together with FLASH help to drive formation of a large (i.e., visible by light microscopy) three-dimensional lattice—the HLB—containing components necessary for efficient transcription and processing of histone mRNA (Figure 10). Gaining additional insight into the biogenesis of NBs will further our understanding of the assembly and function of regulatory machineries required to effectively control gene expression and is crucial to understanding how these complex structures respond to diverse physiological stimuli during normal and pathological circumstances.

## MATERIALS AND METHODS

### Immunofluorescence

For embryos, larval brains, larval salivary glands, and ovaries, the following primary antibodies were used: monoclonal mouse MPM-2 (1:2000; Millipore, Temecula, CA), chicken anti-GFP (1:1000; Millipore), affinity-purified polyclonal rabbit anti-FLASH (1:2000), affinity-purified rabbit and guinea pig anti-Mxc (1:2000; Yang *et al.*, 2009; White *et al.*, 2011), and monoclonal mouse anti-lamin (Developmental Studies Hybridoma Bank, Iowa City, IA). For S2 cells, immunostaining was performed as described (White *et al.*, 2011). The secondary antibodies used (1:2000) in all experiments were goat anti-rabbit immunoglobulin G (IgG) labeled with Alexa Fluor 488 (Abcam, Cambridge, MA) or Cy5 (Jackson, West Grove, PA), goat anti-mouse IgG Cy3 (Jackson), donkey anti-chicken Cy2 (Jackson), and goat anti-guinea pig IgG Cy3 or Cy5 (Jackson). DNA was detected by incubating tissue in 1 μg/ml 4′,6-diamidino-2-phenylindole (DAPI; DAKO, Carpinteria, CA) for 1 min. Embryos were dechorionated, fixed in a 1:1 mixture of 7% formaldehyde:heptane for 20 min, and incubated with primary overnight at 4°C and secondary for 1 h at 25°C. Brains and salivary glands were dissected from third-instar larvae in Grace's medium (Gibco, Grand Island, NY) and fixed in 4% paraformaldehyde and 3.7% formaldehyde, respectively, for 20 min. Brains were permeabilized in 0.2% Tween-20 for 20 min before immunostaining.

### Amylose pull-down assay

The hexahistidine-tagged MBP and MBP-Mxc$^{101}$ proteins (pDest-566 Gateway Destination vector; Addgene plasmid 11517; courtesy of Dominic Esposito, Frederick National Laboratory for Cancer Research, Frederick, MD) were expressed in *E. coli* and subsequently affinity purified through nickel-nitriloacetic acid resin columns (Qiagen, Austin, TX). Fragments of Mxc were labeled with $^{35}$S[Met] by in vitro translation using Promega's TNT coupled rabbit reticulocyte kit (Promega, San Luis Obispo, CA). A 5-μg amount of recombinant MBP proteins was incubated at 4°C with preequilibrated amylose resin (GE Healthcare Life Sciences, Piscataway, NJ) in 100 μl of TEN100 buffer (20 mM Tris, pH 7.5, 0.1 mM EDTA, 100 mM NaCl). Unbound protein was removed by two washes with 250 μl of TEN100. A 10-μl amount of in vitro–translated protein was added to beads along with 10 μl of 10× TEN100 buffer, 14 μl of GDB buffer (10% glycerol, 10 mM dithiothreitol, 0.05 mg/ml bovine serum albumin), and 76 μl of distilled $H_2O$. Proteins were allowed to bind for 2 h at 4°C while being rotated. Amylose beads were washed four times with 1 ml of TEN100 buffer. A 25-μl amount of 2× SDS loading dye (4% SDS, 10% β-mercaptoethanol, 0.125 M Tris, pH 6.8, 20% glycerol, 0.2% bromophenol blue) was added to the beads and boiled for 10 min. The supernatant was loaded onto an SDS–PAGE gel. Gels were stained with Coomassie blue to confirm pull down of recombinant MBP protein. Gels were dried and visualized by autoradiography.

### Imaging

Confocal images for embryo in situ hybridization were obtained at a zoom of 1.0–5.0 with a 20× PlanNeofluar (numerical aperture [NA] 0.5) and 40× PlanApochromat (NA 1.3) objectives using the ZEN data acquisition software on a laser-scanning confocal microscope (510; Carl Zeiss, Heidelberg, Germany). Confocal images for embryo, adult, and larval tissue immunostaining and high-magnification embryo in situ hybridization were obtained at a zoom of 1.0–5.0 with a 63× PlanAchromat (NA 1.4) objective using the ZEN data acquisition software on a laser-scanning confocal microscope (710; Carl Zeiss). Confocal images for *Drosophila* S2 cells were taken at a zoom of 2.0–5.0 with a 40× (NA 1.25) Plan Apochromat objective on a laser-scanning confocal microscope (SP5; Leica, Exton, PA).

For live imaging, transgenic flies harboring GFP-Mxc were generated and crossed to flies carrying a transgenic histone H2Av variant fused to the RFP tag (H2Av-RFP). Female virgins carrying one copy of GFP-Mxc (White *et al.*, 2011) and one of H2Av-RFP (Poulton *et al.*, 2014) were selected and crossed to their male siblings to assure one copy of each transgene maternally supplied to the embryos to be analyzed. Syncytial *Drosophila* embryos were mounted on a lumox porous-surfaced dish (Sarstedt, Numbrecht, Germany) and covered with halocarbon oil 700 (Sigma-Aldrich, St. Louis, MO). Images from the surface of the embryo body were acquired at ~21°C on a Nikon TE2000-E microscope with Visitech Infinity-Hawk multipoint array scanner, using 100× Nikon objectives, a Ludl emission filter wheel with Semrock filters, and Hamamatsu ORCA R2 camera. Excitation was by 491-(GFP) and 561-nm (RFP) lasers. Movies and stills were processed in ImageJ (National Institutes of Health, Bethesda, MD). Fluorescence intensity was calculated for all foci on a single *z*-plane with the highest integrated intensity values in the region of interest. A circle was drawn around each focus and in areas inside five nuclei without fluorescence on the same *z*-plane to be used for background readings. To calculate the corrected total focus fluorescence (CTFF) using ImageJ software, we analyzed data from three embryos representing three independent experiments and used the formula CTFF = integrated density − (area of selected focus × mean fluorescence of background readings) (Burgess *et al.*, 2010; Potapova *et al.*, 2011.

### Embryo in situ hybridization

The *w*$^{1118}$-, *Slbp*$^{15}$-, and *mxc*-mutant embryos were collected and aged at room temperature until they were 8–10 h old. Embryos were fixed in a 1:1 mixture of 7% formaldehyde/heptane for 20 min and rehydrated in 1× phosphate-buffered saline (PBS)/0.1% Tween-20. Histone H3 transcripts were detected by FISH using digoxigenin-labeled H3-coding or H3-ds probe (Lanzotti *et al.*, 2002; White *et al.*, 2007).

### Molecular biology

Mxc fragments used for immunostaining and live-imaging experiments were expressed in *Drosophila* cultured S2 cells or as transgenes in Gateway-compatible vectors (Carnegie Institution, Baltimore, MD) as previously described (White *et al.*, 2011). Mxc fragments used for pull-down assays were all expressed in the pxFRM vector (Lyons *et al.*, 2014). The primers used to amplify all Mxc fragments are listed in Supplemental Table S1.

### Western blotting

Ovary protein lysates were obtained from *w*$^{1118}$; *GFP-Mxc*, *w*$^{1118}$; *GFP-Mxc*$^{LisH\text{-}AAA}$, and *w*$^{1118}$; *GFP-Mxc*$^{SIF\text{-}AAA}$ female flies dissected in 1× Tris PBS. Ovaries were snap-frozen in dry ice and ethanol for 10 min and stored at −20°C overnight. Ovaries were resuspended

in buffer containing 4% SDS and dissociated with 20 strokes of a Dounce homogenizer on ice. Equal amounts of protein were run on a 7.5% acrylamide gel (Bio-Rad, Hercules, CA) and then transferred to a polyvinylidene fluoride membrane (Millipore) presoaked in methanol for 15 min at room temperature. Membranes were incubated overnight at 4°C in primary rabbit anti-GFP (Abcam) antibody to detect GFP-tagged proteins (~250 kDa in size) and in primary mouse anti-lamin (Developmental Studies Hybridoma Bank) antibody to detect *Drosophila* lamin (74 kDa in size). Lamin and an anti-GFP antibody cross-reacting band were used as loading controls. Subsequently membranes were incubated in secondary antibody horseradish peroxidase (HRP)–conjugated donkey-anti rabbit IgG (GE Healthcare Life Sciences) and HRP-conjugated goat-anti mouse IgG (GE Healthcare) for 2 h at room temperature to detect GFP and lamin, respectively. The signal was enhanced using Enhance Signal West Dura (Thermo Scientific, Rockford, IL) and visualized using an 8-MP EX Sigma camera in a BioSpectrum imaging system (UVP) after a 25-min exposure.

### Northern blotting

Northern blotting was performed using a 6% 7 M urea acrylamide gel to resolve histone mRNAs and 7SK RNA (Nguyen *et al.*, 2012) as previously described (Mullen and Marzluff, 2008).

### Statistical analysis

The SEM was calculated by dividing SD by the square root of the number of samples (*n*). Statistical significance between different samples was calculated using the Student's *t* test.

### Computational analysis of Mxc's self-interaction

The structure of the LisH domain of TBL1X (Protein Data Bank ID 2XTC) was identified by HHpred (toolkit.tuebingen.mpg.de/hhpred; Soding, 2005) as a structural template for homology modeling of the LisH domain of Mxc using the Modeller software program (Eswar *et al.*, 2006).

## ACKNOWLEDGMENTS

We are grateful to Mark Peifer for kindly sharing the Nikon TE2000-E microscope (National Institutes of Health Grant R01GM067236), which greatly contributed to our study. We thank Tony Perdue for assistance in microscopy and Zbigniew Dominski and Xiao-cui Yang for generously sharing Mxc and FLASH antibodies. This work was supported by National Institutes of Health Grants F31GM106698-01 to E.T. and R01GM58921 to W.F.M. and R.J.D.

## REFERENCES

Adams JC (2002). Characterization of a Drosophila melanogaster orthologue of muskelin. Gene 297, 69–78.

Aravind L, Landsman D (1998). AT-hook motifs identified in a wide variety of DNA-binding proteins. Nucleic Acids Res 26, 4413–4421.

Bian C, Wu R, Cho K, Yu X (2012). Loss of BRCA1-A complex function in RAP80 null tumor cells. PLoS One 7, e40406.

Bongiorno-Borbone L, De Cola A, Vernole P, Finos L, Barcaroli D, Knight RA, Melino G, De Laurenzi V (2008). FLASH and NPAT positive but not Coilin positive Cajal Bodies correlate with cell ploidy. Cell Cycle 7, 2357–2367.

Bulchand S, Menon SD, George SE, Chia W (2010). Muscle wasted: a novel component of the Drosophila histone locus body required for muscle integrity. J Cell Sci 123, 2697–2707.

Burgess A, Vigneron S, Brioudes E, Labbe JC, Lorca T, Castro A (2010). Loss of human Greatwall results in G2 arrest and multiple mitotic defects due to deregulation of the cyclin B-Cdc2/PP2A balance. Proc Natl Acad Sci USA 107, 12564–12569.

Cerna D, Wilson DK (2005). The structure of Sif2p, a WD repeat protein functioning in the SET3 corepressor complex. J Mol Biol 351, 923–935.

Cortese MS, Uversky VN, Dunker AK (2008). Intrinsic disorder in scaffold proteins: getting more from less. Prog Biophys Mol Biol 98, 85–106.

Deryusheva S, Gall JG (2004). Dynamics of coilin in Cajal bodies of the Xenopus germinal vesicle. Proc Natl Acad Sci USA 101, 4810–4814.

Deryusheva S, Gall JG (2009). Small Cajal body-specific RNAs of Drosophila function in the absence of Cajal bodies. Mol Biol Cell 20, 5250–5259.

Dundr M (2012). Nuclear bodies: multifunctional companions of the genome. Curr Opin Cell Biol 24, 415–422.

Dundr M, Hebert MD, Karpova TS, Stanek D, Xu H, Shpargel KB, Meier UT, Neugebauer KM, Matera AG, Misteli T (2004). In vivo kinetics of Cajal body components. J Cell Biol 164, 831–842.

Dundr M, Misteli T (2001). Functional architecture in the cell nucleus. Biochem J 356, 297–310.

Dundr M, Misteli T (2010). Biogenesis of nuclear bodies. Cold Spring Harb Perspect Biol 2, a000711.

Emes RD, Ponting CP (2001). A new sequence motif linking lissencephaly, Treacher Collins and oral-facial-digital type 1 syndromes, microtubule dynamics and cell migration. Hum Mol Genet 10, 2813–2820.

Eswar N, Webb B, Marti-Renom MA, Madhusudhan MS, Eramian D, Shen MY, Pieper U, Sali A (2006). Comparative protein structure modeling using Modeller. Curr Protoc Bioinformatics Chapter 5, Unit 5.6.

Foray N, Marot D, Gabriel A, Randrianarison V, Carr AM, Perricaudet M, Ashworth A, Jeggo P (2003). A subset of ATM- and ATR-dependent phosphorylation events requires the BRCA1 protein. EMBO J 22, 2860–2871.

Gall JG (2000). Cajal bodies: the first 100 years. Annu Rev Cell Dev Biol 16, 273–300.

Gerlitz G, Darhin E, Giorgio G, Franco B, Reiner O (2005). Novel functional features of the Lis-H domain: role in protein dimerization, half-life and cellular localization. Cell Cycle 4, 1632–1640.

Godfrey AC, Kupsco JM, Burch BD, Zimmerman RM, Dominski Z, Marzluff WF, Duronio RJ (2006). U7 snRNA mutations in Drosophila block histone pre-mRNA processing and disrupt oogenesis. RNA 12, 396–409.

Good MC, Zalatan JG, Lim WA (2011). Scaffold proteins: hubs for controlling the flow of cellular information. Science 332, 680–686.

Harrer M, Luhrs H, Bustin M, Scheer U, Hock R (2004). Dynamic interaction of HMGA1a proteins with chromatin. J Cell Sci 117, 3459–3471.

Hebert MD, Matera AG (2000). Self-association of coilin reveals a common theme in nuclear body localization. Mol Biol Cell 11, 4159–4171.

Kim MH, Cooper DR, Oleksy A, Devedjiev Y, Derewenda U, Reiner O, Otlewski J, Derewenda ZS (2004). The structure of the N-terminal domain of the product of the lissencephaly gene Lis1 and its functional implications. Structure 12, 987–998.

Klingauf M, Stanek D, Neugebauer KM (2006). Enhancement of U4/U6 small nuclear ribonucleoprotein particle association in Cajal bodies predicted by mathematical modeling. Mol Biol Cell 17, 4972–4981.

Knoblich JA, Sauer K, Jones L, Richardson H, Saint R, Lehner CF (1994). Cyclin E controls S phase progression and its down-regulation during Drosophila embryogenesis is required for the arrest of cell proliferation. Cell 77, 107–120.

Kobayashi N, Yang J, Ueda A, Suzuki T, Tomaru K, Takeno M, Okuda K, Ishigatsubo Y (2007). RanBPM, Muskelin, p48EMLP, p44CTLH, and the armadillo-repeat proteins ARMC8alpha and ARMC8beta are components of the CTLH complex. Gene 396, 236–247.

Landais S, D'Alterio C, Jones DL (2014). Persistent replicative stress alters polycomb phenotypes and tissue homeostasis in Drosophila melanogaster. Cell Rep 7, 859–870.

Lanzotti DJ, Kaygun H, Yang X, Duronio RJ, Marzluff WF (2002). Developmental control of histone mRNA and dSLBP synthesis during Drosophila embryogenesis and the role of dSLBP in histone mRNA 3′ end processing in vivo. Mol Cell Biol 22, 2267–2282.

Lanzotti DJ, Kupsco JM, Marzluff WF, Duronio RJ (2004a). string(cdc25) and cyclin E are required for patterned histone expression at different stages of Drosophila embryonic development. Dev Biol 274, 82–93.

Lanzotti DJ, Kupsco JM, Yang XC, Dominski Z, Marzluff WF, Duronio RJ (2004b). Drosophila stem-loop binding protein intracellular localization is mediated by phosphorylation and is required for cell cycle-regulated histone mRNA expression. Mol Biol Cell 15, 1112–1123.

Li Z, Johnson MR, Ke Z, Chen L, Welte MA (2014). Drosophila lipid droplets buffer the H2Av supply to protect early embryonic development. Curr Biol 24, 1485–1491.

Liu JL, Murphy C, Buszczak M, Clatterbuck S, Goodman R, Gall JG (2006). The Drosophila melanogaster Cajal body. J Cell Biol 172, 875–884.

Lyons SM, Ricciardi AS, Guo AY, Kambach C, Marzluff WF (2014). The C-terminal extension of Lsm4 interacts directly with the 3′ end of the histone mRNP and is required for efficient histone mRNA degradation. RNA 20, 88–102.

Ma T, Van Tine BA, Wei Y, Garrett MD, Nelson D, Adams PD, Wang J, Qin J, Chow LT, Harper JW (2000). Cell cycle-regulated phosphorylation of p220(NPAT) by cyclin E/Cdk2 in Cajal bodies promotes histone gene transcription. Genes Dev 14, 2298–2313.

Machyna M, Kehr S, Straube K, Kappei D, Buchholz F, Butter F, Ule J, Hertel J, Stadler PF, Neugebauer KM (2014). The coilin interactome identifies hundreds of small noncoding RNAs that traffic through Cajal bodies. Mol Cell 56, 389–399.

Marzluff WF, Wagner EJ, Duronio RJ (2008). Metabolism and regulation of canonical histone mRNAs: life without a poly(A) tail. Nat Rev Genet 9, 843–854.

Matera AG (1999). Nuclear bodies: multifaceted subdomains of the interchromatin space. Trends Cell Biol 9, 302–309.

Matera AG, Izaguire-Sierra M, Praveen K, Rajendra TK (2009). Nuclear bodies: random aggregates of sticky proteins or crucibles of macromolecular assembly? Dev Cell 17, 639–647.

Menssen R, Schweiggert J, Schreiner J, Kusevic D, Reuther J, Braun B, Wolf DH (2012). Exploring the topology of the Gid complex, the E3 ubiquitin ligase involved in catabolite-induced degradation of gluconeogenic enzymes. J Biol Chem 287, 25602–25614.

Miele A, Braastad CD, Holmes WF, Mitra P, Medina R, Xie R, Zaidi SK, Ye X, Wei Y, Harper JW, *et al*. (2005). HiNF-P directly links the cyclin E/CDK2/p220NPAT pathway to histone H4 gene regulation at the G1/S phase cell cycle transition. Mol Cell Biol 25, 6140–6153.

Mikolajka A, Yan X, Popowicz GM, Smialowski P, Nigg EA, Holak TA (2006). Structure of the N-terminal domain of the FOP (FGFR1OP) protein and implications for its dimerization and centrosomal localization. J Mol Biol 359, 863–875.

Misteli T (2001). The concept of self-organization in cellular architecture. J Cell Biol 155, 181–185.

Misteli T (2005). Concepts in nuclear architecture. Bioessays 27, 477–487.

Mowry KL, Steitz JA (1987). Identification of the human U7 snRNP as one of several factors involved in the 3′ end maturation of histone premessenger RNA's. Science 238, 1682–1687.

Mullen TE, Marzluff WF (2008). Degradation of histone mRNA requires oligouridylation followed by decapping and simultaneous degradation of the mRNA both 5′ to 3′ and 3′ to 5′. Genes Dev 22, 50–65.

Nguyen D, Krueger BJ, Sedore SC, Brogie JE, Rogers JT, Rajendra TK, Saunders A, Matera AG, Lis JT, Uguen P, Price DH (2012). The Drosophila 7SK snRNP and the essential role of dHEXIM in development. Nucleic Acids Res 40, 5283–5297.

Novotny I, Blazikova M, Stanek D, Herman P, Malinsky J (2011). In vivo kinetics of U4/U6.U5 tri-snRNP formation in Cajal bodies. Mol Biol Cell 22, 513–523.

Nussinov R, Ma B, Tsai CJ (2013). A broad view of scaffolding suggests that scaffolding proteins can actively control regulation and signaling of multienzyme complexes through allostery. Biochim Biophys Acta 1834, 820–829.

Parada LA, Sotiriou S, Misteli T (2004). Spatial genome organization. Exp Cell Res 296, 64–70.

Potapova TA, Sivakumar S, Flynn JN, Li R, Gorbsky GJ (2011). Mitotic progression becomes irreversible in prometaphase and collapses when Wee1 and Cdc25 are inhibited. Mol Biol Cell 22, 1191–1206.

Poulton JS, Cuningham JC, Peifer M (2014). Acentrosomal Drosophila epithelial cells exhibit abnormal cell division, leading to cell death and compensatory proliferation. Dev Cell 30, 731–745.

Rajendra TK, Praveen K, Matera AG (2010). Genetic analysis of nuclear bodies: from nondeterministic chaos to deterministic order. Cold Spring Harb Symp Quant Biol 75, 365–374.

Reeves R, Nissen M (1990). The A-T-DNA-binding domain of mammalian high mobility group I chromosomal proteins. J Biol Chem 265, 8573–8582.

Remillieux-Leschelle N, Santamaria P, Randsholt NB (2002). Regulation of larval hematopoiesis in Drosophila melanogaster: a role for the multi sex combs gene. Genetics 162, 1259–1274.

Saget O, Forquignon F, Santamaria P, Randsholt NB (1998). Needs and targets for the multi sex combs gene product in Drosophila melanogaster. Genetics 149, 1823–1838.

Salemi LM, Almawi AW, Lefebvre KJ, Schild-Poulter C (2014). Aggresome formation is regulated by RanBPM through an interaction with HDAC6. Biol Open 3, 418–430.

Salzler HR, Tatomer DC, Malek PY, McDaniel SL, Orlando AN, Marzluff WF, Duronio RJ (2013). A sequence in the Drosophila H3-H4 Promoter triggers histone locus body assembly and biosynthesis of replication-coupled histone mRNAs. Dev Cell 24, 623–634.

Santamaria P, Randsholt NB (1995). Characterization of a region of the X chromosome of Drosophila including multi sex combs (mxc), a Polycomb group gene which also functions as a tumour suppressor. Mol Gen Genet 246, 282–290.

Soding J (2005). Protein homology detection by HMM-HMM comparison. Bioinformatics 21, 951–960.

Strub K, Birnstiel ML (1986). Genetic complementation in the Xenopus oocyte: co-expression of sea urchin histone and U7 RNAs restores 3′ processing of H3 pre-mRNA in the oocyte. EMBO J 5, 1675–1682.

Strzelecka M, Trowitzsch S, Weber G, Luhrmann R, Oates AC, Neugebauer KM (2010). Coilin-dependent snRNP assembly is essential for zebrafish embryogenesis. Nat Struct Mol Biol 17, 403–409.

Sullivan E, Santiago C, Parker ED, Dominski Z, Yang X, Lanzotti DJ, Ingledue TC, Marzluff WF, Duronio RJ (2001). Drosophila stem loop binding protein coordinates accumulation of mature histone mRNA with cell cycle progression. Genes Dev 15, 173–187.

Sun Z, Smrcka AV, Chen S (2013). WDR26 functions as a scaffolding protein to promote Gbetagamma-mediated phospholipase C beta2 (PLCbeta2) activation in leukocytes. J Biol Chem 288, 16715–16725.

Swanhart L, Kupsco J, Duronio RJ (2005). Developmental control of growth and cell cycle progression in Drosophila. Methods Mol Biol 296, 69–94.

Umeda M, Nishitani H, Nishimoto T (2003). A novel nuclear protein, Twa1, and Muskelin comprise a complex with RanBPM. Gene 303, 47–54.

Voronina E, Seydoux G, Sassone-Corsi P, Nagamori I (2011). RNA granules in germ cells. Cold Spring Harb Perspect Biol 3, a002774.

Wei Y, Jin J, Harper JW (2003). The cyclin E/Cdk2 substrate and Cajal body component p220(NPAT) activates histone transcription through a novel LisH-like domain. Mol Cell Biol 23, 3669–3680.

White AE, Burch BD, Yang XC, Gasdaska PY, Dominski Z, Marzluff WF, Duronio RJ (2011). Drosophila histone locus bodies form by hierarchical recruitment of components. J Cell Biol 193, 677–694.

White AE, Leslie ME, Calvi BR, Marzluff WF, Duronio RJ (2007). Developmental and cell cycle regulation of the Drosophila histone locus body. Mol Biol Cell 18, 2491–2502.

Yang XC, Burch BD, Yan Y, Marzluff WF, Dominski Z (2009). FLASH, a proapoptotic protein involved in activation of caspase-8, is essential for 3′ end processing of histone pre-mRNAs. Mol Cell 36, 267–278.

Ye X, Wei Y, Nalepa G, Harper JW (2003). The cyclin E/Cdk2 substrate p220(NPAT) is required for S-phase entry, histone gene expression, and Cajal body maintenance in human somatic cells. Mol Cell Biol 23, 8586–8600.

Zaidi SK, Young DW, Javed A, Pratap J, Montecino M, van Wijnen A, Lian JB, Stein JL, Stein GS (2007). Nuclear microenvironments in biological control and cancer. Nat Rev Cancer 7, 454–463.

Zhao J, Kennedy BK, Lawrence BD, Barbie DA, Matera AG, Fletcher JA, Harlow E (2000). NPAT links cyclin E-Cdk2 to the regulation of replication-dependent histone gene transcription. Genes Dev 14, 2283–2297.